Quaternary Science Reviews 226 (2019) 105998

Contents lists available at ScienceDirect

Quaternary Science Reviews

journal homepage: www.elsevier.com/locate/quascirev

# North Iberian temperature and rainfall seasonality over the Younger Dryas and Holocene

Lisa M. Baldini [a, *], James U.L. Baldini [b], Frank McDermott [c, d], Pablo Arias [e], Marián Cueto [e], Ian J. Fairchild [f], Dirk L. Hoffmann [g, h, i], David P. Mattey [j], Wolfgang Müller [j, k], Dan Constantin Nita [g, l], Roberto Ontañón [e], Cristina Garcíá-Moncó [e], David A. Richards [g]

[a] Department of Geography, Durham University, Science Labs, South Road, Durham DH1 3LE, UK
[b] Department of Earth Sciences, Durham University, Science Labs, South Road, Durham DH1 3LE, UK
[c] UCD School of Geological Sciences, University College Dublin, Belfield, Dublin 4, Ireland
[d] UCD Earth Institute, University College Dublin, Belfield, Dublin 4, Ireland
[e] International Institute for Prehistoric Research of Cantabria, University of Cantabria-Government of Cantabria-Santander, Av. Los Castros 52, Santander, Spain
[f] School of Geography, Earth and Environmental Sciences, University of Birmingham, Edgbaston, Birmingham B15 2TT, UK
[g] School of Geographical Sciences, University of Bristol, University Road, Clifton, Bristol BS8 1SS, UK
[h] CENIEH, Paseo Sierra de Atapuerca s/n, 09002 Burgos, Spain
[i] Department of Human Evolution, Max Planck Institute for Evolutionary Anthropology, Deutscher Platz 6, 04103 Leipzig, Germany
[j] Department of Earth Sciences, Royal Holloway, University of London, Egham, Surrey, TW20 0EX, UK
[k] Institut für Geowissenschaften, Goethe-Universität Frankfurt, Altenhöferallee 1, 60438 Frankfurt am Main, Germany
[l] Faculty of Environmental Science and Engineering, Babes-Bolyai University, Cluj-Napoca, Romania

ARTICLE INFO

*Article history:*
Received 8 March 2019
Received in revised form
20 September 2019
Accepted 11 October 2019
Available online 12 November 2019

*Keywords:*
Holocene
Younger Dryas
Palaeoclimatology
Western Europe
Speleothems
Stalagmites
Oxygen isotopes
Trace elements
Seasonality

ABSTRACT

Several stalagmite records have yielded important but discontinuous insights into northern Iberian climate since the Last Glacial. Here we present the first continuous Iberian stalagmite-based reconstruction of climate since the Bølling-Allerød interstadial, from a single stalagmite sample (GAR-01 from La Garma Cave, Cantabria). The ~13.5 ka GAR-01 record provides the opportunity for replication, continuation, and aggregation of previously published records from northern Spain. The GAR-01 record reveals shifts in oxygen isotope ratios that are inexplicable by appealing to a single control (i.e., exclusively temperature, rainfall amount, etc.). Herein we explore the potential role of rainfall and temperature seasonality shifts on the new $\delta^{18}O$ record using a simple Monte Carlo approach to estimate the seasonal distribution of rainfall and the annual temperature range at 100-year timeslices across the record. This model is corroborated by intervals of monthly-resolved laser ablation trace element data, providing glimpses into past Iberian seasonality shifts. The most salient features of the modelled results include extremely dry Younger Dryas winters (~12.9–11.6 ka BP) and several intervals during the mid-Holocene with almost no summer rainfall (e.g., at 4.2 and 9.0 ka BP). By 1.6 ka BP, a near-modern rainfall seasonality was established. According to the modelling results, seasonal rainfall and temperature distribution variability can account for 95% of the record. The model presented here provides a new tool for extracting critical missing seasonality information from stalagmite $\delta^{18}O$ records. Intervals where the model does not converge may represent transient climate anomalies with unusual origins that warrant further investigation.



## 1. Introduction

The Iberian Peninsula is located in a climatologically important location at the western periphery of Europe. The region's climate is sensitive to the phase of the North Atlantic Oscillation (NAO) (Rodrigo et al., 2000; Trigo et al., 2004) as well as oceanic heat advection to the North Atlantic due to Atlantic Meridional Overturning Circulation (AMOC) variability (Mary et al., 2017). The Iberian Peninsula is affected by both Atlantic and Mediterranean

* Corresponding author.
*E-mail address:* l.m.baldini@durham.ac.uk (L.M. Baldini).

https://doi.org/10.1016/j.quascirev.2019.105998

influences (Gimeno et al., 2010), and therefore the entire peninsula does not experience identical climate shifts at the same time; instead climate shifts are spatiotemporally variable. However, the proximity of northern Iberia to the climatologically-important oceanic subpolar and subtropical gyres (that transfer heat and salt toward the Nordic seas) (Morley et al., 2011; Pérez-Brunius et al., 2004) and the Azores High (that partially controls the position and strength of westerly winds and the North Atlantic Oscillation) (Baker et al., 2015; Olsen et al., 2012; Trouet et al., 2009; Walczak et al., 2015) means that climate records from the region are particularly sensitive to major modes of atmospheric and oceanic circulation that also affect the rest of Europe and the entire Northern Hemisphere. The coastal region north of the Cantabrian Mountains exhibits particularly robust and stationary relationships between the NAO state and winter rainfall amount, at least over the most recent 100-year period for which climate reanalysis data are available (Comas-Bru and McDermott, 2014). AMOC variability, linked via teleconnections to the Intertropical Convergence Zone (ITCZ), also affects the region's climate (e.g., Pohlmann et al., 2006; Souza and Cavalcanti, 2009). North Iberia is therefore an ideal location to study both temporal shifts in AMOC as well as NAO-driven changes in temperature and precipitation.

However, this same sensitivity to several key European climate forcings also complicates the interpretation of north Iberian climate proxy records. This issue is compounded by the fact that the controls on the climate signal within any one proxy are temporally variable. A number of high-quality climate records exist that use terrestrial archives distributed across northern Iberia, and these have helped shed light on this issue. In particular, the region's extensive karst has permitted the development of a series of excellent stalagmite-based proxy records of temperature (Martin-Chivelet et al., 2011), rainfall (Moreno et al., 2017; Railsback et al., 2011; Smith et al., 2016), and the $\delta^{18}O$ composition of North Atlantic surface water (Domínguez-Villar et al., 2009). Recently, a number of publications have highlighted that the complex and sometimes contradictory pattern of climate proxy results observed could stem from shifting seasonality in rainfall (Morellon et al., 2009; Moreno et al., 2010, 2017; Walczak et al., 2015), potentially due to meridional displacement of the Azores High which broadly tracked insolation and mean North Atlantic climate state. Specifically, research has highlighted the possibility that climate change on the Iberian Peninsula is the result of time-transgressive seasonality changes across the region (Moreno et al., 2017). Different cave sites and stalagmite samples are variably sensitive to local environmental factors, and consequently the absence of a single continuous record from a single stalagmite covering the entire Holocene and into the last glacial complicates efforts to isolate the seasonality signal inherent within north Iberian climate.

Here we present new decadal-scale oxygen isotope data for a U-series dated stalagmite from La Garma Cave in north Iberia covering the entire Holocene. These new data, combined with previously published data from the same stalagmite over the interval from 10.5 to 13.5 ka BP, provide a rare continuous record of Iberian climate since the Bølling-Allerød interstadial from a single stalagmite sample. Consequently, the new isotope dataset provides the opportunity for replication, continuation, and aggregation of previously published shorter but otherwise high-quality Younger Dryas and Holocene speleothem records from northern Spain (Domínguez-Villar et al., 2008, 2009; Dominguez-Villar et al., 2017; Martin-Chivelet et al., 2011; Moreno et al., 2010, 2017; Railsback et al., 2011; Rossi et al., 2018; Stoll et al., 2009). The oxygen isotope results are clearly not explicable by appealing to a single control (i.e., exclusively temperature, rainfall amount, etc.). We therefore explore the potential role of seasonality shifts in rainfall on the new $\delta^{18}O$ record by developing a new modelling technique that uses the oxygen isotope data to estimate rainfall and temperature seasonality shifts across the Holocene and into the late Pleistocene. This model is corroborated by intervals of laser ablation trace element data obtained at a monthly resolution, which provide direct glimpses into past seasonality shifts. The new data and model presented here are discussed in both site-specific and regional contexts, and, in combination with other published records from the Atlantic margin of Europe, offer new insights into Iberian climate evolution from the late Pleistocene. Specifically, modelled seasonal temperature and rainfall shifts provide a framework for the interpretation of other proxy records.

## 2. Site description

La Garma Cave (43°25′N, 3°40′W) is developed within lower Cretaceous limestones on several levels within a 187 m high hill situated 11 km ESE of Santander, northern Spain (Fig. 1a). The cave's entrance is located ~5 km inland from the Bay of Biscay at 85 meter above sea level (m.a.s.l.). This cave site is well studied, and a detailed site description is available in previous publications (Arias, 2009; Arias et al., 2001, 2011; Arias and Ontañón, 2012; Baldini et al., 2015). The current vegetation above the cave consists of dense $C_3$ vegetation, including kermes oak, hazel, bay, and eucalyptus (Rudzka-Phillips et al., 2013). Soil thickness varies, but is typically about 1 m. Meteorological data for the Santander Airport Global Network of Isotopes in Precipitation (GNIP) station (43°29′28° N; 3°48° W; 52 m.a.s.l.), located 13 km west of La Garma Cave, indicate a mean annual air temperature of 14.78 °C and a mean total annual precipitation of 870 mm from 2000 to 2010, and the Köppen–Geiger climate classification is 'warm temperate' (Comas-Bru and McDermott, 2014). The Santander Airport GNIP station also provides over a decade of monthly precipitation $\delta^{18}O$ ($\delta^{18}O_p$) data. An analysis of longer rainfall records (from 1912 C.E.) from several local meteorological stations (Santander/Parayas, Villaverde de Pontones, and Santander Ojaiz) suggests that the GNIP data were measured during a slightly drier than average interval of the last 100 years, with mean rainfall values from these stations suggesting a long-term (1912–2011 AD) mean annual rainfall of ~1228 mm compared with a mean annual rainfall of 1109 mm during the same interval as the GNIP data (2000–2010 AD). Here we use the GNIP data because it is coupled with rainfall $\delta^{18}O$ data and temperature data.

The Santander GNIP monthly $\delta^{18}O_p$ data (2000–2010 AD) exhibit a clear annual cycle with maximum values (ranging from −3.89 to −3.55‰ V-SMOW) from May to August and minimum values (−6.79 to −6.07‰) between October and March (Supplementary Fig. S1). Based on Spearman's rank ($r_s$) correlation analysis, monthly $\delta^{18}O_p$ values are significantly positively correlated with mean monthly temperature values ($r_s = 0.56$; $p < 0.001$; $n = 130$). Although monthly $\delta^{18}O_p$ values are also significantly negatively correlated with mean monthly rainfall amount ($r_s = -0.56$; $p < 0.001$; $n = 130$), this correlation is a statistical artefact where the rainfall amount versus $\delta^{18}O$ relationship is controlled by very high $\delta^{18}O$ values coinciding with very low summer rainfall values, which ultimately simply reflect high summer temperatures. An analysis of months with similar temperatures confirms that most of the rainfall isotope signal is driven by temperature. According to Gimeno et al. (2010), seasonal moisture source changes also play a role in determining the seasonal $\delta^{18}O_p$ cycle; the $^{18}O$-enriched Mediterranean is the dominant moisture source for the Iberian Peninsula during the summer, whereas in winter moisture is sourced from the relatively less $^{18}O$-enriched Atlantic region. In addition, previous studies have noted the role of

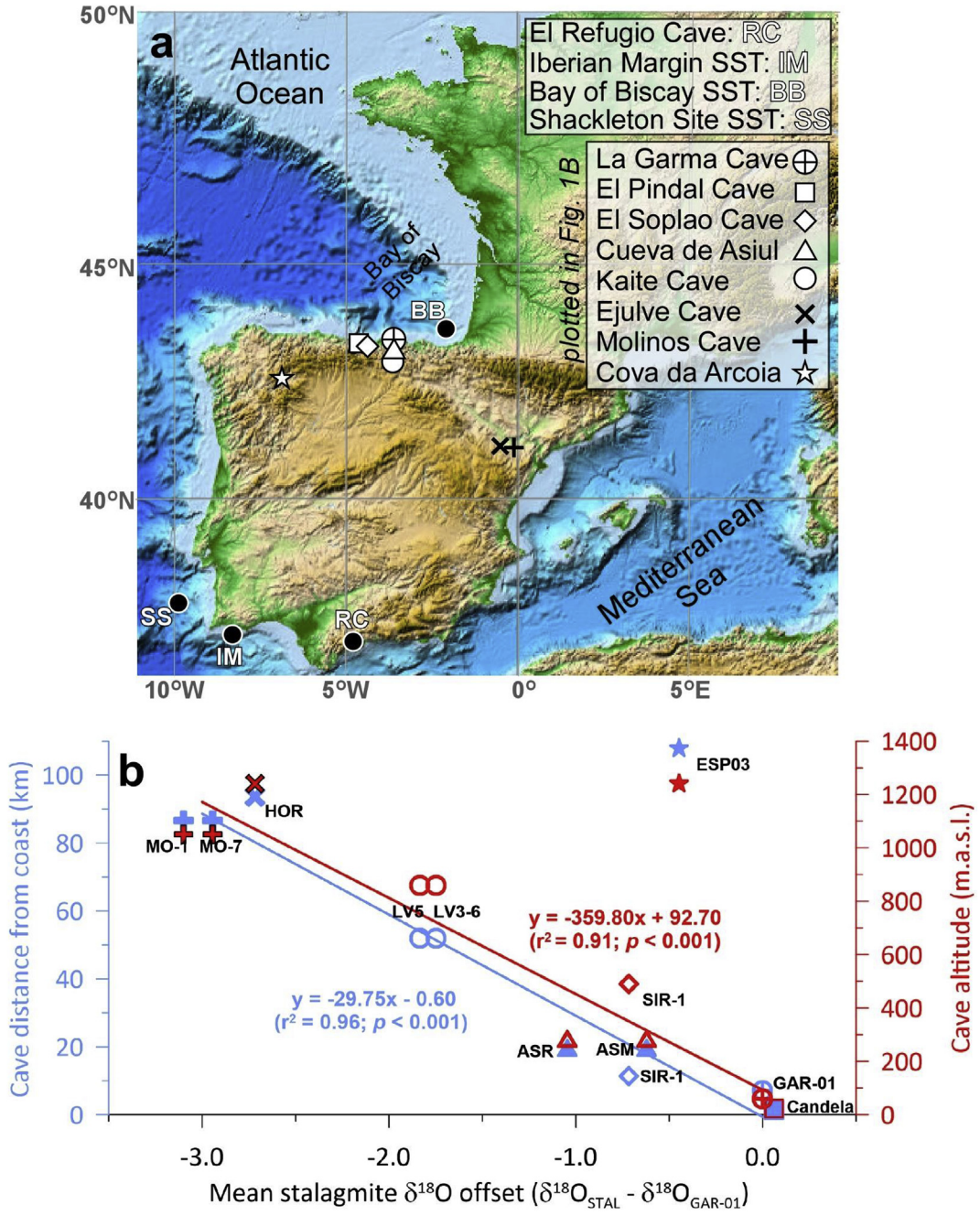


**Fig. 1.** a) Digital elevation map showing the relative position of cave sites and marine sediment core SST records discussed in the text: Iberian Margin (Bard, 2002); Bay of Biscay (Mary et al., 2017); Shackleton Site (Ausin et al., 2019). b) Relationship between the mean stalagmite $\delta^{18}O$ offset (e.g., the difference between the mean $\delta^{18}O$ of a regional stalagmite ($\delta^{18}O_{STAL}$) minus the $\delta^{18}O$ of GAR-01 ($\delta^{18}O_{GAR-01}$) averaged over the same interval of growth). All caves identified in 1a are presented in 1b except El Refugio cave for which $\delta^{18}O$ data are not available. In b, cave symbols are coloured according to whether the mean $\delta^{18}O$ offset is compared to the cave's distance to the closest coast (blue symbols) or altitude (red symbols). All cave mean $\delta^{18}O$ offset values except those for Cova da Arcoia were used to calculate the blue and red regression lines and associated equations.

North Atlantic Oscillation in modulating northern Iberian temperature, rainfall amount, and rainwater $\delta^{18}O_p$ (Baldini et al., 2008; Moreno et al., 2014; Trigo et al., 2004); thus, the La Garma Cave stalagmite $\delta^{18}O$ record also reflects low frequency variability in North Atlantic westerlies, temperature, and rainfall seasonality partially driven by the NAO. Ultimately, for seasonal climates such as northern Iberia with a mean annual temperature >10 °C, stalagmite $\delta^{18}O$ records are most likely to record recharge-weighted precipitation $\delta^{18}O$ (Baker et al., 2019), which for our site is predominantly a consequence of temperature and moisture source.

## 3. Methods

### 3.1. Sample GAR-01 description and preparation

Stalagmite GAR-01 consists entirely of coarsely crystalline calcite and was collected in two parts on separate occasions in 2004 from the cave's Lower Gallery. The Holocene portion of GAR-01 (GAR-01A) was found lying on the cave floor adjacent to the actively growing portion of the same stalagmite (GAR-01B), which was collected. Sectioning revealed that recent calcite was deposited

non-conformably on top of older growth within GAR-01B (Fig. 2). Subsequent U-Th dating revealed that GAR-01A was broken from its growth position during the Middle Ages, and represents the middle interval of the adjacent, actively growing stalagmite GAR-01B that was still in situ. Archaeological analysis and 18 AMS radiocarbon dates of charcoal (n = 11) and human bone (n = 5) samples collected from the Lower Gallery of La Garma Cave suggest humans visited the location at least twice within the period 688–754 C.E. (Ontañón et al., 2018), consistent with stalagmite U-Th ages for the break. The cave contains numerous stalagmites that were broken during the Middle Ages for unknown reasons, many of which have actively re-grown since the breakage, resulting in post-Middle Ages calcite deposition atop the broken bases. The physically separated but intrinsically linked samples GAR-01 A and B are collectively referred to as stalagmite GAR-01 in the text, unless specifically referring to either of the two physically discrete samples. Stalagmite GAR-01 grew continuously from ~14.0 ka to the date of collection in 2004 and represents 800 mm of total growth with a 57 μm $yr^{-1}$ mean extension rate. Both GAR-01A and B were sectioned, polished, cleaned, and sampled using a conventional dental drill at a resolution of ~38 years per sample. The results of high-resolution (sub-decadal) laser ablation analysis for C and O isotopes over the Younger Dryas interval was reported previously (Baldini et al., 2015).

### 3.2. GAR-01 stable isotope analysis

Conventionally drilled powder samples (drilled at a 2.2 mm spatial resolution) were analysed using a GV Instruments Multiflow-Isoprime systems at Royal Holloway University, London (RHUL). Herein, the GAR-01 $\delta^{18}O$ record will be discussed in detail. Previous research has shown stalagmite $\delta^{13}C$ to be sensitive to

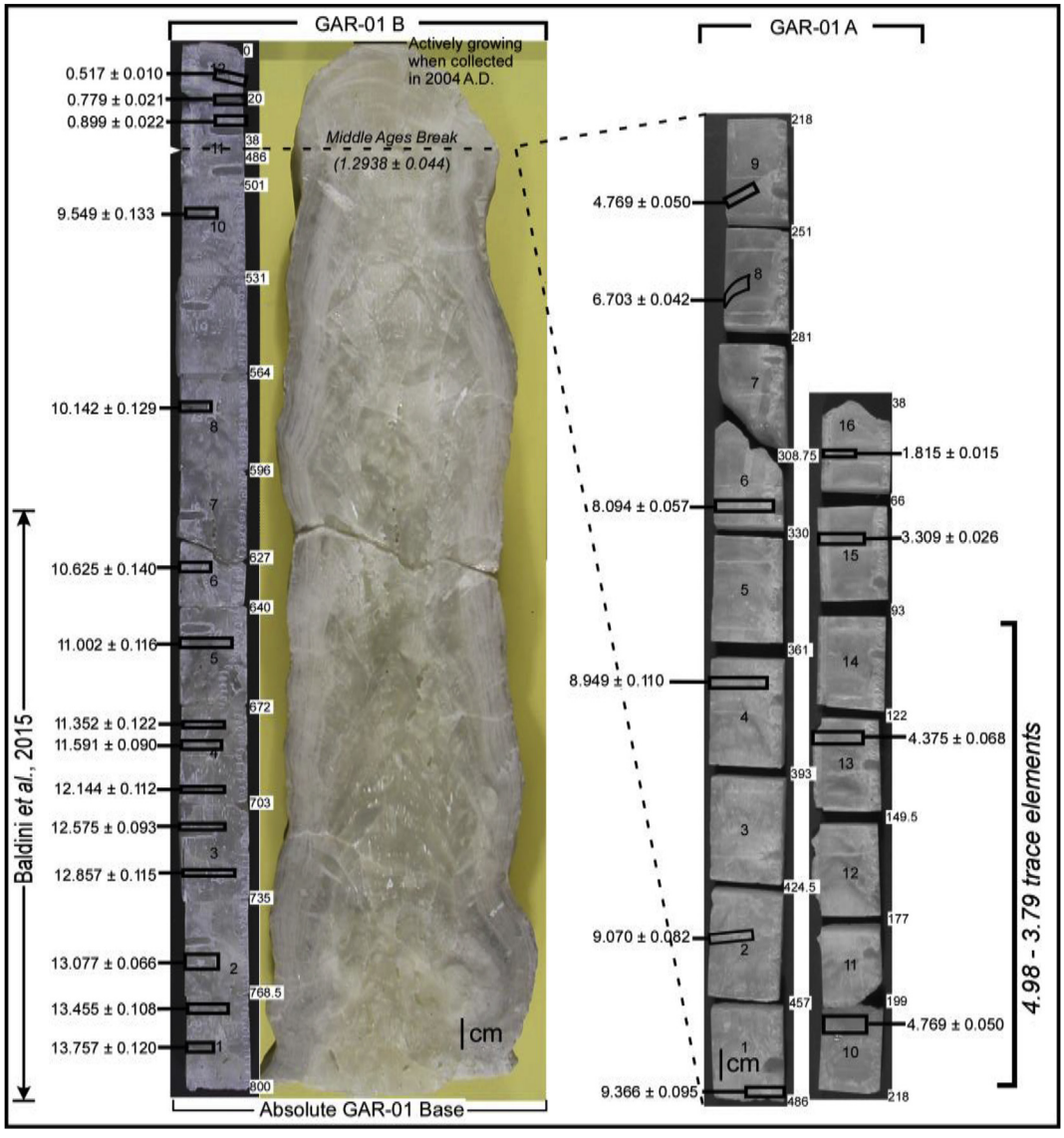


**Fig. 2.** Stalagmite GAR-01 A & B with U-Series sample locations (black boxes) and corresponding ages (in ka BP 1950). U-Series powders were drilled at regular intervals along the length of GAR-01. GAR-01 A was the first section of stalagmite GAR-01 to be collected and dated. GAR-01 A was broken off by Middle Ages visitors to the cave and discovered on the ground adjacent to the in situ portion of GAR-01 (GAR-01 B) in 2003. Thus stalagmite GAR-01 A constitutes the Holocene and GAR-01 B constitutes a record of the pre-Holocene with Middle Ages break and post-Middle Ages growth to present-day. The lower portion of GAR-01 B was the subject of a previous study that yielded a high resolution reconstruction of the Younger Dryas Event (Baldini et al., 2015). GAR-01 (GAR-01 A and GAR-01 B) grew continuously from 13.864 ka BP to the date of collection in 2004. Some brief breaks in the record exist where a rock saw was used to slab the stalagmite for LA-ICPMS analysis.

land-use changes at the surface (e.g., Baldini et al., 2005). Archaeological investigations at La Garma Cave over several decades by P. Arias and colleagues suggests that human activities (e.g., deforestation, fortifications, etc.) have intermittently modified the surface environment through the Holocene. Due to the potential for these activities to overprint the $\delta^{13}C$ climate signal, an in-depth discussion of the GAR-01 $\delta^{13}C$ record is considered outside the scope of the current study but will form the basis of a future paper on anthropogenic activity at the site.

### 3.3. LA-ICPMS analysis

A 193-nm wavelength excimer LA-ICPMS system at RHUL (RESOlution M-50 prototype coupled to an Agilent 7500ce quadrupole ICP-MS) featuring a two-volume Laurin LA cell was used to produce a high-resolution Mg dataset across select intervals of the stalagmite. Trace element data were obtained as continuous profiles using a rectangular spot ($285 \times 12\ \mu m$) at a $10\ \mu m\ s^{-1}$ sample movement and a 15 Hz laser repetition rate, producing an effective spatial resolution of ~15 μm, which is approximately monthly-scale for fast growing intervals of GAR-01 during the mid-Holocene. $^{43}Ca$ concentrations were used as an internal standard and NIST612 as external standard (Müller et al., 2009).

### 3.4. U-Th dating and age model development

Twenty-four powder samples were drilled from within distinct growth layers along the central growth axis of GAR-01 using a handheld drill and a tungsten carbide drill bit for uranium series dating. Chemical separation and purification of uranium and thorium and their subsequent isotopic analysis using a Thermo-Finnigan Neptune multicollector inductively coupled mass spectrometer (MC-ICP-MS) at the University of Bristol followed the techniques and procedures outlined by Hoffmann et al. (2007). Measured $^{238}U$ concentrations in stalagmite GAR-01 ranged between 71.2 and 118.7 ng $g^{-1}$, and the measured $^{230}Th/^{232}Th$ activity ratio varied between 22.1 and 2089.9. All ages were calculated using the decay constants reported in Cheng et al. (2000) and corrected for detrital contamination assuming a bulk earth ($^{238}U/^{232}Th$) activity ratio of 0.746 (Hans Wedepohl, 1995) and ($^{230}Th/^{238}Th$) = ($^{234}U/^{238}U$) (Table S1).

All 24 U-Th dates from GAR-01 are in stratigraphic order (Table S1) and a distance-age model was generated using the COPRA (Constructing Proxy Record from Age models) algorithm (Breitenbach et al., 2012). For the previously published Younger Dryas record, we used the StalAge algorithm to calculate the age model (Baldini et al., 2015), but here considering the proxy record with translated age model uncertainties facilitates comparisons to the large number of shorter existing records, and COPRA has this capability. Although both the COPRA and StalAge algorithms construct age models using Monte Carlo simulations to interpolate between U-Th ages and account for potential outliers, age inversions, and potential hiatuses, StalAge does not yet translate the age model uncertainties to the proxy record. Additionally, the StalAge mean age model for the full GAR-01 record contained short intervals where the StalAge model produced unrealistically high growth rates (Supplementary Fig. S2). For these reasons we elected to use the COPRA algorithm in the present study. However, the two age models agree very well overall, particularly over the Younger Dryas interval (Supplementary Fig. S2). Based on 24 $^{230}Th$ dates, the 2004 C.E. date of collection, and the COPRA output, stalagmite GAR-01 grew continuously from 13.861 ka until it was collected in 2004 C.E. (Fig. 3 and Supplementary Table S1). Based on the age model, the conventional drill $\delta^{18}O$ dataset discussed herein has a mean temporal resolution of 37.9 years.

### 3.5. Cave monitoring

Air temperatures were monitored at four different locations within La Garma Cave from July 2006 to July 2007 using TinyTag temperature loggers (Jackson, 2009), including at the location from which stalagmite GAR-01 was collected. Monitored cave air temperatures at all of the La Garma Cave monitoring sites are 1.38−2.70 °C lower than those of the surface meteorological measurements. The elevation of the monitored cave passage (59 m.a.s.l.) is close to that of the meteorological station (52 m.a.s.l.) and therefore altitude cannot account for this difference. Three of the monitored sites in the cave recorded air temperatures with extremely small variations through the year (annual range < 0.22 °C). However, air temperature at the GAR-01 site has a higher annual range of 0.69 °C (from a maximum monthly mean value of 12.37 °C in November and a minimum of 11.68 °C in February), and a long-term mean temperature value of 12.08 °C. This is 2.70 °C colder than the mean outside temperature, and reflects cave ventilation systematics and a winter cold air trap, common to temperate cave sites (Bourges et al., 2001; James et al., 2015; Sherwin and Baldini, 2011), that disproportionately affects the GAR-01 site.

As previously reported (Baldini et al., 2015), drip samples were obtained during monthly site visits to La Garma cave between September 2004 and October 2005. Monthly-integrated dripwater samples were collected from: i) the feeder drip site to stalagmite GAR-01 (GDW-1) and ii) a drip site (GDW-2) located 3 m from drip site GDW-1. Dripwater samples were collected using 1 L graduated collection vessels to allow the mean drip rate to be calculated for each period of collection. More recently (June 2012 to November 2013), and to augment the monthly-scale drip rate data, a Stalagmate® drip logger was deployed at the GAR-01 drip site to monitor drip rate at 30-min intervals over 18 months. All dripwater samples were analysed for oxygen and hydrogen isotope compositions. All drip water isotope analyses were performed at the Nevada Stable Isotope Laboratory, University of Nevada-Reno (UNR) using a Micromass Aquaprep device interfaced to a Micromass dual inlet IsoPrime stable isotope ratio mass spectrometer and the Epstein and Mayeda (1953) $CO_2$-$H_2O$ equilibration method. Dripwater $\delta^{18}O$ results are reported in units of per mil (‰) versus Vienna Standard Mean Ocean Water (VSMOW) with uncertainties of ±0.10‰ (1σ) based on replicate analyses of the UNR dripwater oxygen isotope internal reference standard for water.

## 4. Results and discussion

### 4.1. Rainfall and dripwater $\delta^{18}O$

Stalagmite GAR-01 was fed by a seasonal drip on the basis of a maximum discharge rate of $4.09 \times 10^{-7}\ L\ s^{-1}$ and a coefficient of variation of 55.5 (i.e., calculated as the absolute value of the standard deviation divided by the mean drip rate multiplied by 100) following the Smart and Friederich (1987) classification scheme. Stalagmate® drip logger data (collected between June 2012 and November 2013) revealed that the GAR-01 drip site (GDW-1) drips continuously (i.e., never drying completely) and exhibits long-term seasonal trends with daily drip rates of 131 drips per day in June 2012 decreasing to a minimum of 75 drips per day in winter 2012. For the period of study, GDW-1 monthly-integrated dripwater $\delta^{18}O$ and $\delta D$ values ranged from −5.95 to −5.07‰ and −33.10 to −26.60‰ (VSMOW), respectively, and were considerably restricted in range compared to monthly Santander rainwater isotope ratios recorded between 2003 and 2005 ($\delta^{18}O$: 7.85 to −2.04‰; $\delta D$: 45.93 to −11.88‰) (Fig. 4a). The amount-weighted mean GDW-1 drip water $\delta^{18}O$ (WM $\delta^{18}O = -5.73$‰) was calculated

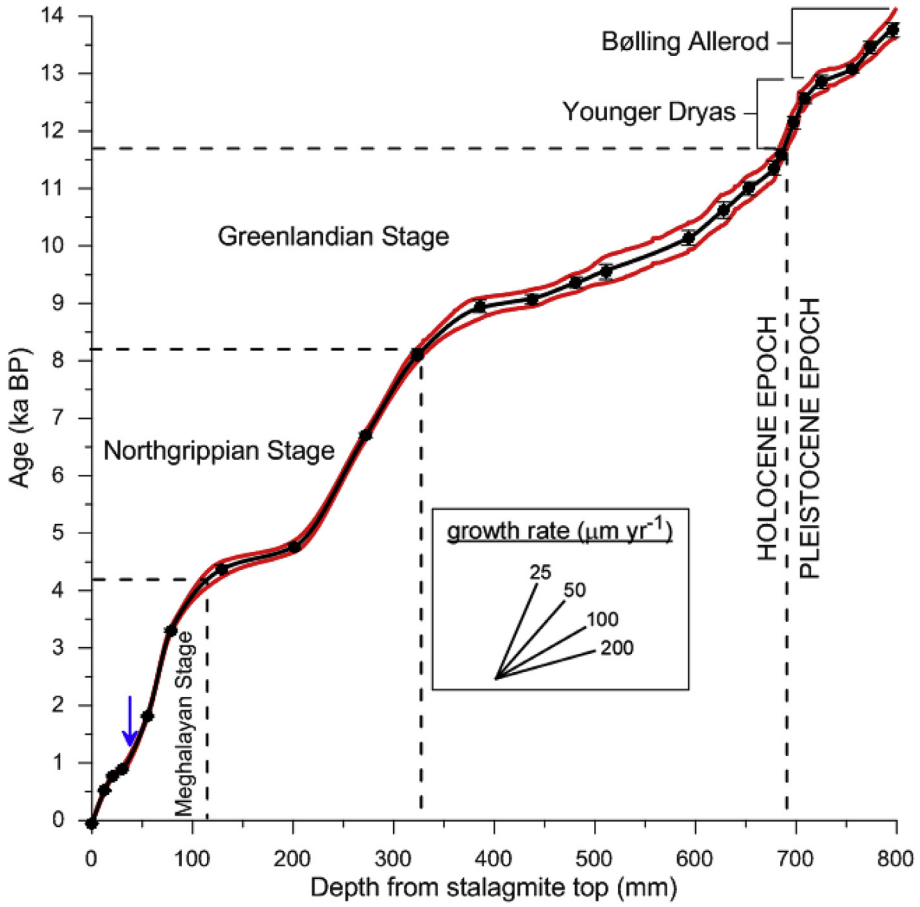


**Fig. 3.** COPRA (Breitenbach et al., 2012) mean age model for stalagmite GAR-01. Age with 95% confidence bands (red lines) constrained by 24 $^{230}$Th dates (black dots with 2σ error bars). Recently ICS-defined Holocene Stages referred to in the text are identified as are the pre-Holocene Younger Dryas and Bølling-Allerød events discussed in detail previously (Baldini et al., 2015). The mean growth rate over the Holocene was 59 μm yr$^{-1}$. Intervals with particularly rapid growth rates are observed during the late Northgrippian stage (between 4.7 and 4.2 ka BP: 156 μm yr$^{-1}$) and during the Greenlandian stage (between 10.4 and 8.7 ka BP: 149 μm yr$^{-1}$). The intervals of slowest growth occur during the Younger Dryas (discussed in detail in Baldini et al. (2015)) and during the mid-Meghalayan stage (between 3.2 and 1.8 ka BP: 14.6 μm yr$^{-1}$).

for March to October 2005 (e.g., corresponding to the period during which collected dripwater volume was directly measured) (Fig. 4b). This GDW-1 $\delta^{18}O_{WM}$ value is 0.99‰ lower than the Santander precipitation WM $\delta^{18}O$ recorded over the same period (−4.74‰) but more similar to the Santander precipitation WM $\delta^{18}O$ recorded seven months prior (e.g., between August 2004 and March 2005; −5.53‰) (Fig. 4a, d). A 7.5 month dripwater residence time is suggested by $\delta^{18}O$ data from monitored drip site GDW-2 (3 m from GDW-1) for which a lag of this length is observed between dripwater $\delta^{18}O$ and Santander rainwater $\delta^{18}O$ minima (Fig. 4c). The muted dripwater $\delta^{18}O$ variability relative to the Santander precipitation WM $\delta^{18}O$ variability requires long-term mixing of percolating water within the vadose zone, and an indicative (non-unique) mass balance calculation suggests that mixing of rainwater from 2003 to 2004 in the proportions 40:60 (respectively) could produce the observed mean drip-water value during 2005. Shallow soil water $\delta^{18}O$ values from a previous study indicate that rainwater mixing and homogenisation is completed within the upper 1.5 m of soil (Comas-Bru and McDermott, 2015). Based on the results of drip water monitoring (e.g., the drip rate minimum occurs during the rainiest season (winter) and the temporal lag observed between rainwater and dripwater isotopes), a mean residence time of 6–7.5 months likely exists within this well-mixed karst reservoir (Baldini et al., 2015) (Fig. 4).

The mean GDW-1 dripwater $\delta^{18}O$ value (−5.61‰, V-SMOW) combined with the $\delta^{18}O$ value of the calcite that forms the most recent deposition on stalagmite GAR-01 (−3.93‰, V-PDB; the last drill analysis point, centred around 1976 C.E.) were used to assess the extent to which GAR-01 calcite was deposited in oxygen isotopic equilibrium with its dripwater. Under perfect equilibrium conditions, the temperature calculated on the basis of equilibrium water-calcite fractionation factors should approximate the observed modern cave air temperature. However, considerable debate exists in the literature regarding the most appropriate water-calcite oxygen isotope fractionation factor for speleothem calcites (e.g., Demeny et al., 2010; Fairchild and Baker, 2012; Johnston et al., 2013; McDermott, 2004; McDermott et al., 2011; McDermott et al., 2006; McDermott et al., 2005; Tremaine et al., 2011), and even regarding the extent to which the equilibrium concept is applicable to stalagmites (Daëron et al., 2019). Use of the Kim and O'Neill (Kim and O'Neill, 1997; Kim et al., 2007) equation yields a temperature of only 6.3 °C, much lower than the measured mean cave air temperature at the GAR-01 site (c. 12 °C), reflecting the well-known tendency for this equation to yield apparent cave temperatures that are much too low (e.g., McDermott et al., 2005). By contrast, the empirical equation of Tremaine et al. (2011), based on 'farmed' speleothems at multiple locations within Hollow Ridge Cave (Florida), indicates a value of 10.6 °C, a little lower than the measured cave air temperature. The equations of Coplen (2007) and Demeny et al. (2010) yield values that are higher (13.29 °C)

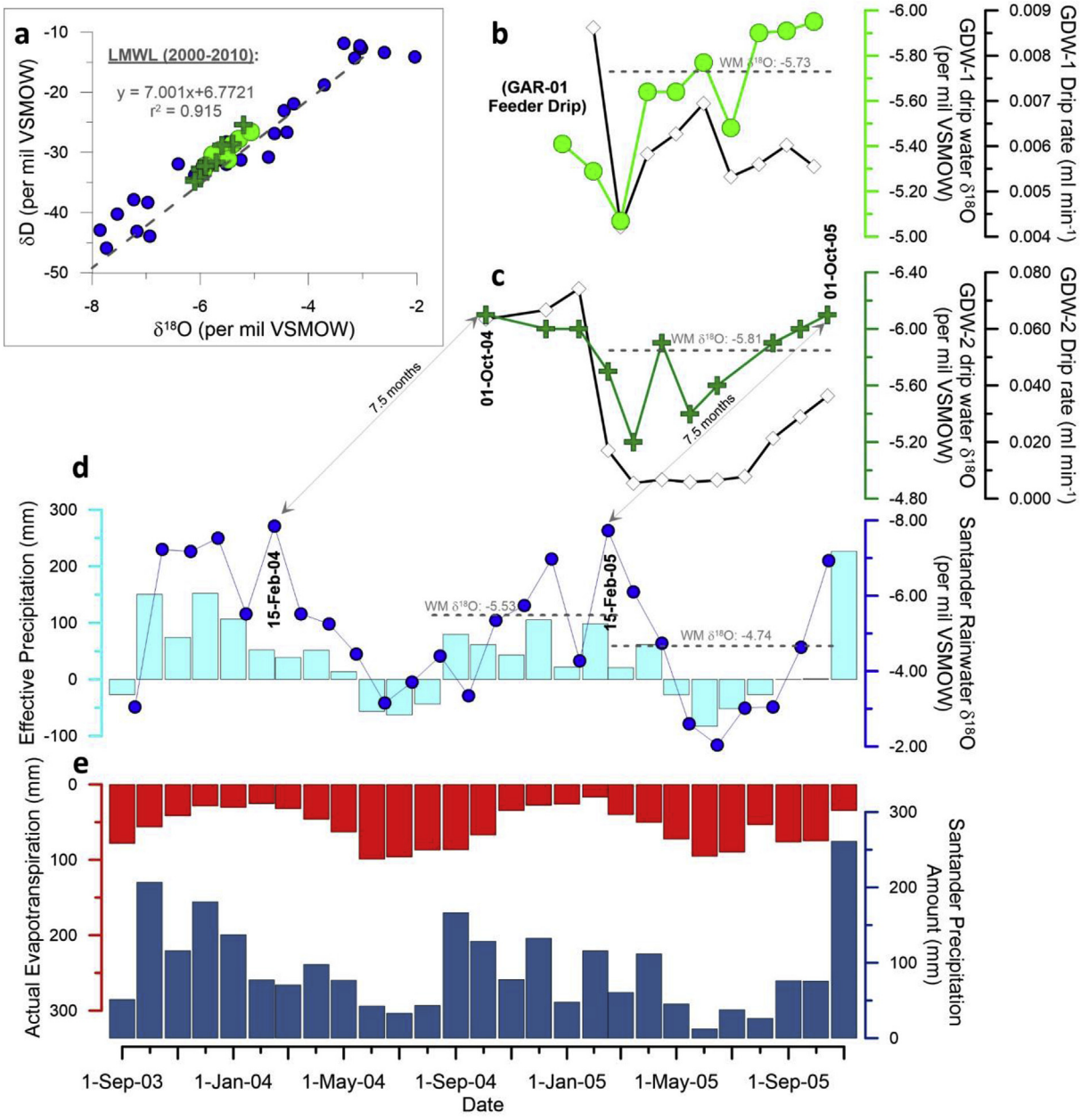


**Fig. 4.** La Garma Cave monitoring data and local climate variability during the study period. A) Stable isotopes of monthly Santander rainwater sampled between September 2003 and November 2005 (blue circles) and La Garma cave drip water from drip sites, GDW-1 (feeder drip to stalagmite GAR-01; light green circles) and GDW-2 (a drip site 3 m away from GDW-1; green crosses) sampled during the study period. B, C) Dripwater isotope data for GDW-1 (light green circles) and GDW-2 (green crosses) compared to contemporaneous estimates of drip rate (based on dividing the volume of drip water collected by the period of collection) through time. D) Variability in effective precipitation (an estimate of the net hydrological balance) and Santander rainwater $\delta^{18}O$ during the study period. E) Variability in monthly actual evapotranspiration and Santander precipitation amount during the study period. Actual evapotranspiration and effective precipitation were calculated using the modified Thornthwaite (Thornthwaite, 1955) and Grindley (Grindley, 1969) methods. Horizontal dashed grey lines indicate the amount-weighted mean (WM) of drip water $\delta^{18}O$ for GDW-1 (−5.73‰) and GDW-2 (−5.81‰) between March and October 2005 (the period of time when dripwater volume data was obtained) and WM Santander precipitation $\delta^{18}O$ (−4.74‰) between March and October 2005 (for ease of comparison with WM dripwater $\delta^{18}O$). The WM Santander precipitation $\delta^{18}O$ (−5.53 ‰) between August 2004 and March 2005 is also shown. The arrows in the figure indicate a probably lag (7.5 months) in dripwater response to meteoric precipitation. (Figure updated from Baldini et al. (2015)).

and lower (9.0 °C) than the observed cave air temperature, respectively. Clearly it is not possible to be definitive about the extent to which cave carbonates are precipitated in oxygen isotopic equilibrium and our perception of equilibrium depends on the somewhat arbitrary choices of fractionation factors from the literature. Regardless, the fractionation factor based on 'cave-farmed' speleothems (Tremaine et al., 2011) is found to most closely approximate the observed cave air temperature at La Garma, suggesting that this is most appropriate for GAR-01 calcite deposition.

### 4.2. The GAR-01 $\delta^{18}O$ record

#### 4.2.1. Controls on GAR-01 stable isotope data

Numerous factors influence stalagmite $\delta^{18}O$ values, including temperature (both regional external air temperature and in-cave air temperature), rainfall amount (the 'amount effect'), moisture source isotopic composition, rainfall seasonality, and moisture mass trajectory, with temperature and trajectory dominating the signal in northern Iberia. Correspondingly, variability across the

Younger Dryas (YD) interval in GAR-01 was previously interpreted as primarily reflecting external temperature (i.e., low regional temperatures driving meteoric precipitation $\delta^{18}O$ and consequently calcite $\delta^{18}O$ to lower values) with moisture source region and trajectory shifts playing a secondary role (Baldini et al., 2015). According to Baldini et al. (2015), a temperature decrease of 6–9 °C during the YDE compared to Bølling-Allerød (B-A) temperatures could explain the 3.1‰ lowering of $\delta^{18}O$ during the event. Elevated ocean water $\delta^{18}O$ and lower in-cave temperatures characteristic of that time interval would have forced the GAR-01 $\delta^{18}O$ record higher, so cannot explain the observed decrease, although both may have offset the observed decrease somewhat. Similarly, sea level rose ~40 m across the YD from 14 to 11 ka BP (Grant et al., 2014), and a more distal shoreline similarly cannot explain the lower values. However, the new 14 ka-long GAR-01 record presented here reveals $\delta^{18}O$ values during several intervals within the Holocene (an epoch characterised by warm conditions in northern Iberia) that are similar to those observed during the YD (Mary et al., 2017). For example, in the decadally-resolved GAR-01 $\delta^{18}O$ dataset, the $\delta^{18}O$ at 8.974 ka BP is −5.08‰, compared to a value of −5.01‰ at 12.29 ka BP at the height of the YD; similarly the $\delta^{18}O$ at 4.709 ka BP is −5.00‰ (Fig. 5). The Iberian Margin sea surface temperature (SST) record from off the SW coast of Iberia (39°11′ N, 10°0′ W) suggests a mean early Holocene SST of ~19 °C (Bard, 2002, 2003; Pailler and Bard, 2002a, b) compared with a YD low of ~13 °C. A SST record from the Bay of Biscay (Mary et al., 2017) suggests that north Iberian temperatures at ~4.7 ka BP were ~14.9 °C, warmer than the modern values from the same core of 14.7 °C, and almost certainly warmer than YD values (the Bay of Biscay SST record does not extend to the YD). This is also consistent with other regional records (such as Greenland ice core temperature proxy records) indicating that the low $\delta^{18}O$ values present at that time within the GAR-01 record are not interpretable purely in terms of temperature.

Based on modern-day monitoring at the GAR-01 drip site, GAR-01 $\delta^{18}O$ reflects rainwater $\delta^{18}O$ but with variability that is attenuated by long-term (monthly-to annual-scale) mixing and storage within the vadose zone. Drip rate monitoring data over a 1.5-year period suggests that the GAR-01 $\delta^{18}O$ record is not seasonally biased but rather reflects continuous, year-round deposition. Continuous year-round stalagmite deposition is supported by the following lines of evidence: i) The GAR-01 feeder drip (GDW-1) was continuously monitored for 1.5 years and drip rate never decreased below 75 drips per day, ii) attenuation of the dripwater $\delta^{18}O$ relative to rainwater $\delta^{18}O$ suggests a well-mixed reservoir, iii) GAR-01 has a columnar and crystalline structure with an absence of visible laminae (Fig. 2), and iv) the ~6–7.5 month residence time (Fig. 4) combined with a lack of dissolution cups in the stalagmite morphology suggests that the drip at no time becomes undersaturated with respect to calcite.

#### 4.2.2. GAR-01 stable isotope data across the Holocene

The GAR-01 conventionally drilled $\delta^{18}O$ data between 13.345 ka BP and 2004 C.E. ranged from −5.08 to −3.34‰ (mean = −4.37‰, $\sigma = 0.31$‰) (Fig. 5b). For clarity, the Holocene GAR-01 record is subdivided into the following three Holocene stages as recently defined by the International Commission on Stratigraphy (ICS) (Cohen et al., 2013; Walker et al., 2012): i) Greenlandian (**11.7 to 8.2 ka BP**), ii) Northgrippian (**8.2 to 4.2 ka BP**), and iii) Meghalayan (**4.2 ka BP to Present**). During the Greenlandian stage (**11.7 to 8.2 ka BP**), the most conspicuous feature is a decreasing trend in the GAR-01 $\delta^{18}O$ data from −3.84‰ at 11.7 ka BP to −4.99‰ at 8.2 ka BP (Fig. 5). The most pronounced negative excursion during this interval occurs at ~9 ka BP and may reflect the north Iberian climatic

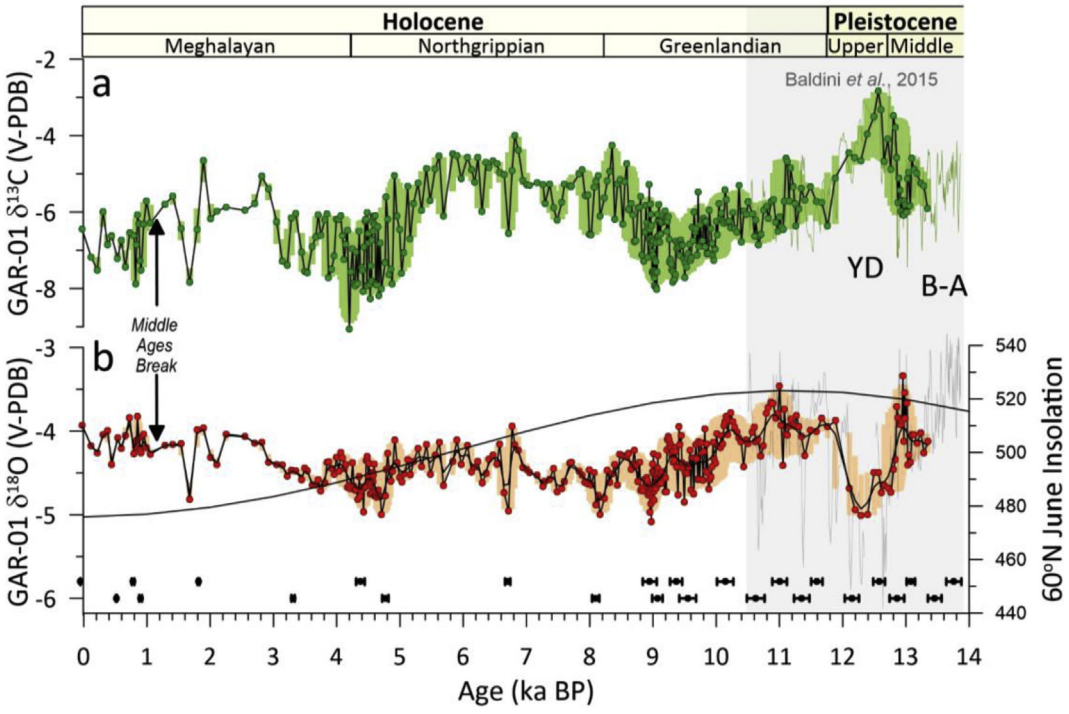


**Fig. 5.** The decadal-scale hand-drilled GAR-01 $\delta^{13}C$ (green circles) and $\delta^{18}O$ (red circles) datasets spanning 13.3445 ka BP to 2004 C.E. (when the sample was collected) are shown with the COPRA-calculated 2.5 and 97.5% quantile confidence intervals ($\delta^{13}C$-green shading; $\delta^{18}O$-orange shading). Also shown is the previously published GAR-01 laser $\delta^{18}O$ data (grey lines) between 13.66 and 10.5 ka BP (Baldini et al., 2015). GAR-01 U-Series ages (solid black circles) with 2σ error bars are also shown. The Younger Dryas (YD), Bølling-Allerød (B–A), Middle Ages Break (see text and Fig. 2) and the corresponding geologic epochs and stages are also noted on the figure. The 60°N June insolation curve (Berger and Loutre, 1991) is shown for comparison and highlights the combined role of insolation and millennial to sub-millennial forcing events in modulating the GAR-01 $\delta^{18}O$ record.

response to the previously documented '9.2 ka event'. Detected in numerous climate proxy records across the Northern Hemisphere (Fleitmann et al., 2008; Genty et al., 2006; Masson-Delmotte et al., 2005; Rasmussen et al., 2007), the '9.2 ka event' may reflect the effects of a meltwater pulse (MWP) (Fleitmann et al., 2008). The event is also observed in a stalagmite record from Dongge Cave in China (Dykoski et al., 2005), suggesting that it also influenced the East Asian Summer Monsoon. Interestingly, the expression of the 9.2 ka event in GAR-01 is similar in magnitude to the GAR-01 YD $\delta^{18}O$ anomaly (Baldini et al., 2015) with $\delta^{18}O$ values of −5.08 and −5.00‰, respectively (Fig. 5). Previous research suggests that conditions in northern Spain were likely considerably warmer and wetter at ~9 ka BP (Morellón et al., 2018) relative to the YD and this is consistent with relatively rapid GAR-01 growth rates observed during the early Holocene (Fig. 3). The '8.2 ka event' is evident in the GAR-01 $\delta^{18}O$ record at 8.16 ka BP as a −0.7‰ anomaly (relative to the Holocene mean of −4.37‰) but is relatively muted in comparison to the negative GAR-01 $\delta^{18}O$ anomaly at ~9 ka BP. This is potentially due to the stalagmite's slower growth rate at 8.2 ka BP (Fig. 3) resulting in higher temporal averaging per data point. A distinct double-pronged $\delta^{18}O$ anomaly centred on 8.345 and 8.216 ka BP was detected in stalagmite LV5 from Kaite Cave and interpreted as the response to two major MWPs that lowered North Atlantic seawater isotope ratios (Domínguez-Villar et al., 2009). Like LV5, but unlike stalagmite SIR-1 from El Soplao cave (Rossi et al., 2018), the GAR-01 record also features a double-pronged $\delta^{18}O$ anomaly. Possible growth hiatuses (e.g., Asiul Cave − ASR; El Soplao Cave − SIR-1) and erosional surfaces (e.g., Cova da Arcoia - ESP03) in other samples from north Iberia suggest that the event affected the entire region.

The Northgrippian (**8.2 to 4.2 ka BP**), is characterised by an increase in $\delta^{18}O$ values from 8.2 to 6.8 ka BP of 1.05‰ (Fig. 5). From 6.7 to 4.2 ka BP, $\delta^{18}O$ values decrease by 0.73‰ with the lowest values of this stage observed at 6.17 (−4.95‰), 4.7 (−4.99‰), and 4.4 (−4.96‰) ka BP (Fig. 5). At 4.2 ka BP, $\delta^{18}O$ values increase to −4.38‰ (similar to the Holocene mean) and values remain similar to, or slightly elevated above, the Holocene mean until 3.87 ka BP. This interval potentially reflects the well-documented '4.2 ka Event' that was previously attributed to abrupt cooling of the North Atlantic potentially linked to a Bond Event (Bond et al., 1997; Bond et al., 1999); however, the isotope response within GAR-01 is relatively subdued. Our data suggests that the shift to drier conditions at 4.2 ka BP at this North Atlantic maritime site was muted compared to the pronounced aridification that occurred across other drier areas (Carolin et al., 2019; Isola et al., 2019; Staubwasser et al., 2003). This interpretation is further supported by the relatively rapid GAR-01 growth rate across the latter 500 years of the Northgrippian stage (Fig. 3). The Meghalayan stage (**4.2 ka BP to 2004 C.E.**) in stalagmite GAR-01 is characterised by a 0.45‰ negative shift between 4.0 ka BP and 3.7 ka BP followed by a gradual increasing trend to −3.96‰ (at 1.8 ka BP). From 1.8 ka BP until the sample was collected, $\delta^{18}O$ values oscillate about a mean of - 4.15‰ (slightly higher than the Holocene mean). At 1.67 ka BP, the GAR-01 $\delta^{18}O$ and $\delta^{13}C$ records (Fig. 5) exhibit a pronounced negative anomaly (−0.67 and −1.13‰, respectively) that is not associated with any known climatic event, nor is it replicated in regional records (Fig. 6). Thus, we tentatively ascribe the anomaly to site-specific factors (e.g., a localised climate shift or hydrological event) rather than a regional scale climate event.

#### *4.2.3. GAR-01 $\delta^{18}O$ compared with other north Iberian stalagmite records*

Numerous previously published stalagmite records from northern Spain (Domínguez-Villar et al., 2008, 2009; Dominguez-Villar et al., 2017; Martin-Chivelet et al., 2011; Moreno et al., 2010, 2017; Railsback et al., 2011; Rossi et al., 2018; Smith et al., 2016; Stoll et al., 2009) provide valuable overlapping data coverage and a degree of replication for sections of the GAR-01 Holocene time-series (Fig. 6). In Fig. 6, regional stalagmite $\delta^{18}O$ records were normalised to the mean GAR-01 $\delta^{18}O$ record over the respective intervals of overlap to facilitate comparison. Overall, much of the centennial to millennial scale $\delta^{18}O$ variability observed in these other stalagmites is in excellent agreement with that in GAR-01 (Figs. 6 and 7). The mean $\delta^{18}O$ offset ($\delta^{18}O_{STAL} - \delta^{18}O_{GAR\text{-}01}$) between GAR-01 and regional records ($\delta^{18}O_{STAL}$) largely reflects differences in cave altitude and distance from the coast (Fig. 1b). Stalagmites from all sites plot along statistically significant negative linear regression lines when the mean $\delta^{18}O$ offset is compared to cave distance from the coast ($y = -29.75x - 0.60$; $r^2 = 0.96$, $p < 0.001$) and altitude ($y = -359.80\,x + 92.70$; $r^2 = 0.91$, $p < 0.001$) except the ESP03 record from Cova da Arcoia that has mean $\delta^{18}O$ offset (−0.45‰) relative to GAR-01 that is higher than expected given the cave's high altitude and distance from the coast (Fig. 1b). The slope of the isotope ratio versus altitude line is similar to that calculated by de Oliveira and da Silva Lima (2010) in their study of northwest Iberian rainfall oxygen isotope relationships.

Stalagmite Candela from El Pindal Cave (4°30′W, 43°23′N, 24 m.a.s.l) (Moreno et al., 2010) exhibits the lowest mean $\delta^{18}O$ offset (0.06‰) relative to the GAR-01 mean over the same growth intervals (Figs. 1b and 6). The low mean $\delta^{18}O$ offset between La Garma and El Pindal stalagmites is attributed to the similar geographic setting of these caves (i.e., low elevation and within a few kilometres of the north Iberian coast) (Fig. 1). Stalagmite ESP03 from Cova da Arcoia (42°37′N, 7°05′W, 1240 m.a.s.l) (Railsback et al., 2011) exhibits an offset of only −0.45‰ despite the cave's relatively high altitude and distance from the coast (the predicted offset based on Fig. 1b would be ~ -3 to −3.5‰). This is potentially attributed to Cova da Arcoia's more westerly location with an increased influence of westerly-derived $^{18}O$-enriched marine aerosols relative to more easterly sites. Alternatively, it may also reflect occasional seasonal (winter) undersaturation of drip water, consequently not preserving low $\delta^{18}O$ winter rainfall, an interpretation broadly consistent with several episodes of erosion evident in stalagmite ESP03 across the Holocene (Railsback et al., 2011). Stalagmite SIR-1 from El Soplao Cave (43° 17′ 46.23″N, 4° 23′ 37.21″W, 490 m.a.s.l) (Rossi et al., 2018) and stalagmites ASM and ASR from Cueva de Asiul (43°19′N, 3°35′W, 285 m.a.s.l) (Smith et al., 2016) exhibit mean $\delta^{18}O$ offsets of −0.72‰ (SIR-1), −0.62‰ (ASM), and −1.04‰ (ASR) relative to overlapping mean GAR-01 $\delta^{18}O$. El Soplao and Cueva de Asiul are situated at higher elevation and further inland from the coast than La Garma Cave, explaining much of the observed $\delta^{18}O$ offset (Fig. 1b). The composite stalagmite record (LV3, LV4, LV5, and LV6) and LV5 (only) from Kaite Cave (43°2′N, 3°39′W, 860 m.a.s.l) (Domínguez-Villar et al., 2008, 2009) exhibit mean $\delta^{18}O$ offsets of −1.75 and −1.83‰, respectively. The mean $\delta^{18}O$ offset between Kaite stalagmites and GAR-01 is largely attributable to the altitude difference (Kaite is ~700 m higher) and Kaite Cave's greater distance from the coast (~50 km inland) (Fig. 1 b). Ejulve (40°45′31″N; 0°35′8″W, 1240 m.a.s.l) and Molinos (40°47′33″N; 0°26′57″W; 1050 m.a.s.l) (Moreno et al., 2017) stalagmites (HOR, MO-1, and MO-7) exhibit the highest mean $\delta^{18}O$ offset compared to GAR-01 with values of −2.72‰, −3.10‰, and −2.94‰, respectively. Moreno et al. (2017) did not previously interpret their Molinos and Ejulve cave stalagmite $\delta^{18}O$ data due to a lack of understanding of the factors driving the observed $\delta^{18}O$ variability. Although we do not interpret the Molinos and Ejulve stalagmite $\delta^{18}O$ variability here, the overall offset in mean $\delta^{18}O$ values relative to GAR-01 is potentially due to the greater altitude

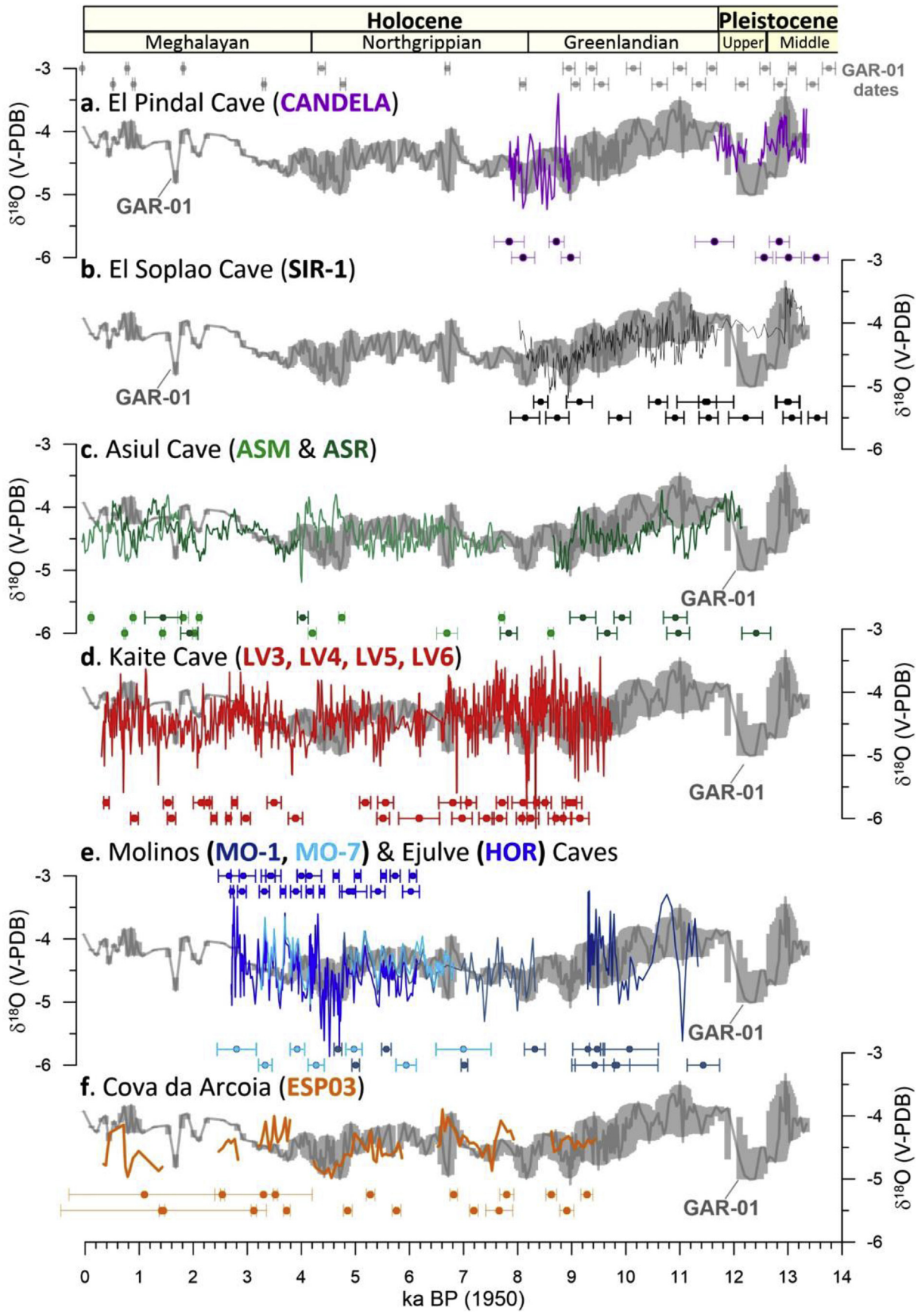


**Fig. 6.** Stalagmite GAR-01 $\delta^{18}O$ (grey line in each panel) time series data compared to shorter overlapping isotope datasets from published northern Spanish stalagmite records: a) Stalagmite Candela from El Pindal Cave (purple line; Moreno et al., 2010); b) Stalagmite SIR-1 (black line) from El Soplao Cave (Rossi et al., 2018); c) Stalagmites ASM (green line) and

and distance from the coast of Molinos and Ejulve caves relative to La Garma Cave (Fig. 1b).

To determine the relationship between regional and GAR-01 $\delta^{18}O$ records, all datasets were linearly interpolated using the *Regular Interpolation* (linear) function within the statistics software PAST v. 3.x (Hammer et al., 2001) and temporally overlapping intervals were compared using Spearman's rank correlation analysis. On decadal timescales regional $\delta^{18}O$ datasets are significantly but weakly correlated with GAR-01 $\delta^{18}O$, despite the strong visual match (Fig. 7). The lack of stronger correlations is probably due to chronological uncertainties and a generally low signal-to-noise ratio characteristic of Holocene climate (Figs. 6 and 7). For instance, GAR-01 is negatively correlated with Asiul stalagmite ASM (Spearman's rank correlation coefficient ($r_s$) = - 0.20, $p < 0.001$) whilst ASR from the same cave exhibits a significant positive correlation ($r_s = 0.24$, $p < 0.001$) with GAR-01 (Fig. 7). Additionally, stalagmites ESP03 and GAR-01 are significantly positively correlated ($r_s = 0.21$, $p < 0.001$) over the pre-4 ka BP portions of these records but the large dating uncertainties of the ESP03 record over the Meghalayan (i.e., the Late Holocene) prevent statistical comparison over that interval (Fig. 7). Besides dating uncertainties, other factors potentially responsible for the weak correlations observed between GAR-01 $\delta^{18}O$ and regional records at decadal timescales include site-specific differences (e.g., varying hydrologies lending certain samples more or less sensitive to transient climate events (Baldini et al., 2006)) and possible aliasing effects (e.g., differences in the temporal resolution of sampling; Baldini et al., 2008). Although GAR-01 and Katie Cave's LV5 record exhibit similar variability ($r_s = 0.20$, $p < 0.01$) between 8.545 and 6.905 ka BP (with both detecting a two-pronged 8.2 ka BP event), the overall correlation of Kaite cave stalagmites (LV3 − 6) with GAR-01 is quite low ($r_s = 0.09$, $p < 0.01$). This is potentially due to chronological uncertainties, or alternatively to Kaite Cave's location on the southern (leeward) slopes of the Cantabrian Mountains that form a hydrological/meteorological divide between northern and central Spain (Fig. 1a).

## 5. A palaeoseasonality model

### 5.1. Model set-up

As discussed previously, the variability within the GAR-01 $\delta^{18}O$ record is not reasonably attributable exclusively to mean annual temperature shifts. In particular, low values of ~ -5‰ found at 12.29 ka BP (the height of the cold YD), at 8.974 ka BP (regional warmth), and at 4.709 ka BP (regional warmth) cannot have the same origin. However, it is conceivable that seasonality changes in both rainfall and temperature may have contributed to these common low values. To investigate this further, we have developed a simple model that uses a Monte Carlo approach to estimate the seasonal distribution of rainfall as well as the annual temperature range. The model assumes that annual mean regional outside temperature is represented by the Iberian Margin temperature record (Bard, 2002, 2003) adjusted for regional temperature differences (Table S2). The correlation between modern surface air temperatures between the nearest meteorological stations to both sites (La Garma Cave and the Iberian Margin core site) is very high (Fig. S3). The Mary et al. (2017) Bay of Biscay SST record is more proximal and higher resolution than the Iberian Margin record (Fig. 1a), but does not extend into the YD, and is therefore compared with the output of the model rather than as an input. Modern temperatures at the La Garma Cave site are ~3 °C cooler than at the Iberian Margin core location, consequently modelled MAT outside the cave is corrected by 3 °C compared with the Iberian Margin SST record. The annual in-cave temperature is set as 2.7 °C colder than the regional mean annual outside temperature. Whereas at many sites in-cave temperature reflects the outside MAT, at La Garma Cave monitoring reveals the presence of a 'cold trap' that exaggerates the importance of winter outside air temperatures (see Section 3.5). Monthly modelled temperatures are linked to the outside mean annual temperature via modern empirical relationships between annual mean, maximum, and minimum temperature values observed at the Santander GNIP station. The modern annual temperature range (e.g., seasonality) increases only slightly with decreasing temperature, and is controlled by the positive relationship between the mean annual air temperature and the minimum and maximum temperature, respectively, in which the minimum temperature is more sensitive to changes in the mean annual temperature (Table S2). The model permits a randomly generated maximum increase or decrease in annual temperature range of 1 °C; in other words, minimum and maximum temperatures derived from the Iberian Margin SST record are allowed to randomly vary by between −0.5 and 0.5 °C each, and consequently the maximum range introduced into the modelled temperature output range above and beyond that observed in the Iberian Margin SST record is 1 °C. Consequently, the modelled MAT also has a maximum randomness of 1 °C. Because the maximum randomness in temperature range introduced by the model is limited to 1 °C, the model returns whether the seasonal temperature range increases or decreases, but may underestimate the actual increase in seasonality. The model assumes that the same relationship between meteoric precipitation $\delta^{18}O$ and temperature observed at the nearest GNIP station (Santander, 13 km to the west of the site) holds true through the entire GAR-01 record (see Table S2 for a detailed list of parameters and steps used in the model).

Next, the model creates a seasonal rainfall distribution of random polarity and amplitude. In other words, the model produces a randomly generated seasonal cycle in rainfall that could range from an extremely wet winter but arid summer, to an extremely arid winter but wet summer, to extremely muted seasonality (i.e., an even distribution of rainfall through the year). The model then produces an amount weighted annual mean meteoritic precipitation $\delta^{18}O$ value, considers mixing within the vadose zone, and produces a $\delta^{18}O$ value for modelled dripwater. The model then uses the empirical Tremaine equation (Tremaine et al., 2011) to model GAR-01 calcite $\delta^{18}O$ ($\delta^{18}O_{mod}$) precipitated from drip water $\delta^{18}O$. The Tremaine equation was chosen over other equations based on thermodynamic principles because in-cave kinetic effects are implicitly accounted for, but the model output is reasonably insensitive to the drip water-calcite fractionation equation used.

ASR (dark green line) from Cueva de Asiul (Smith et al., 2016); d) The composite Kaite cave record (stalagmites LV3, LV4, LV5, and LV6; red line) (Domínguez-Villar et al., 2008; 2009); e) Stalagmites MO-7 (light blue line) and MO-1 (dark blue line) from Molinos Cave and stalagmite HOR (royal blue line) from Ejulve Cave (Moreno et al., 2017); f) Stalagmite ESP03 from Cova da Arcoia (orange line; Railsback et al., 2011). All stalagmite isotope datasets were normalised to the GAR-01 record over the respective intervals of overlap to account for regional differences in rainfall $\delta^{18}O$ induced by altitude, distance from the coast, and karst reservoir effects (effectively resulting in a shift along the y-axis). The variability of each record is unchanged. The original means for each of the normalised datasets/GAR-01 for the same time interval are as follows for $\delta^{18}O$: a) Candela/GAR-01 (8.98−7.84 ka BP) = −4.64‰/-4.59‰, Candela/GAR-01 (12.231−11.640 ka BP) = −4.21‰/-4.26‰, Candela/GAR-01 (13.344−12.455 ka BP) = −3.96‰/-4.14‰; b) SIR-1/GAR-01 (13.864−8.031 ka BP) = −5.01‰/-4.21‰; c) ASM/GAR-01 (7.769 to −0.061 ka BP) = −5.05‰/-4.44‰; ASR/GAR-01 (12.153−0.498 ka BP) = −5.43‰/-4.39‰; d) Kaite Composite/GAR-01 (9.745−0.3045 Ka BP) = −6.21‰/-4.47‰; e) MO-1/GAR-01 (11.335−4.727 ka BP) = −7.43‰/-4.33‰, MO-7/GAR-01 (6.812−3.253 ka BP) = −7.38‰/-4.43‰; f) ESP03/GAR-01 (9.44−0.34 ka BP) = −4.92‰/-4.47‰ (see also Fig. 1b). Grey shading represents the 95% proxy uncertainty bounds produced by COPRA for the GAR-01 record. U-Series dates and 2σ errors are shown for each record (colours as above).

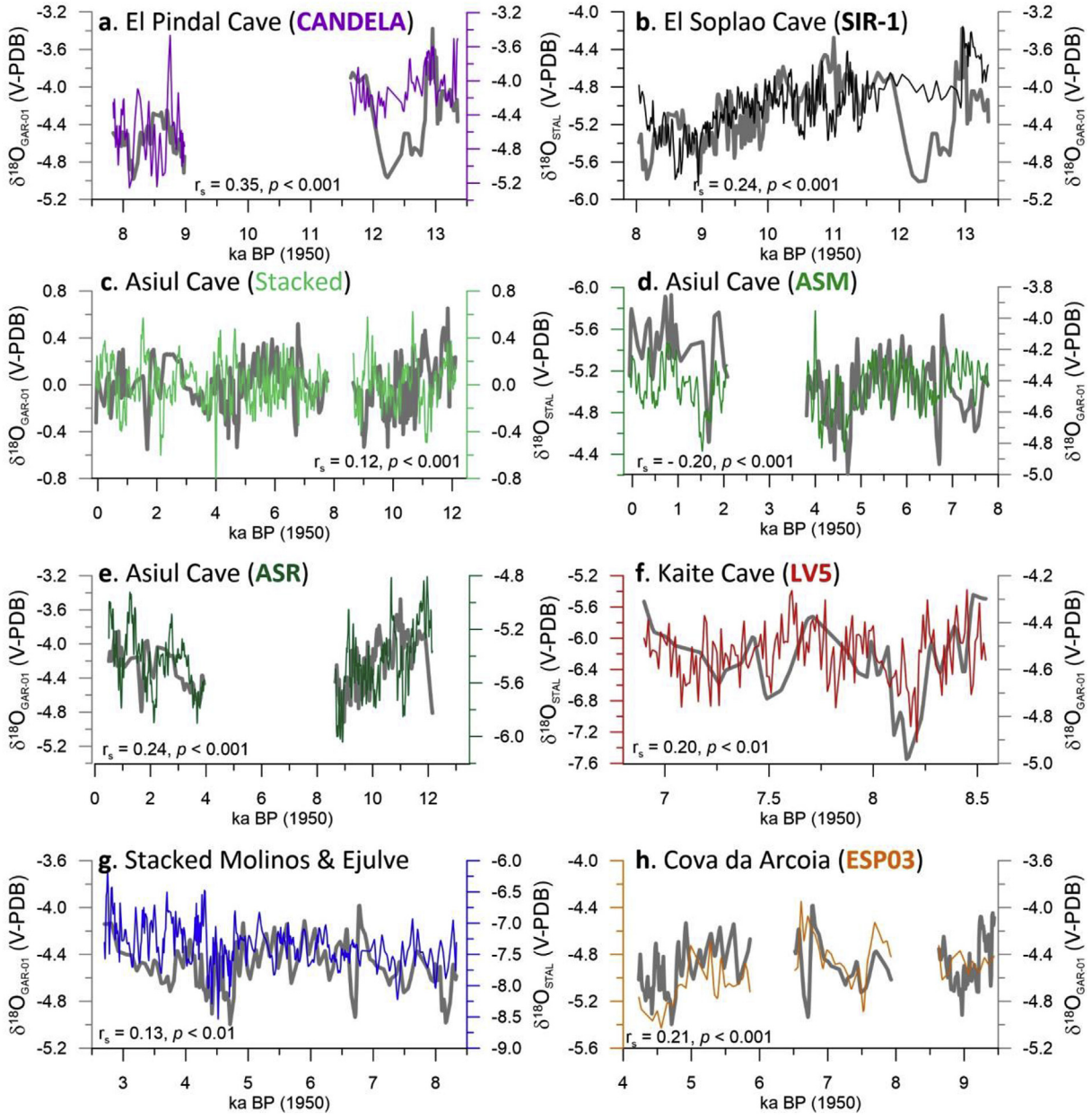


**Fig. 7.** Panels illustrating the relationship between individual records and GAR-01 in more detail than Fig. 6. Results of Spearman's rank correlation analysis of the decadally-interpolated $\delta^{18}O$ profiles of stalagmite GAR-01 (thick grey line) are included within each panel: '$\delta^{18}O_{GAR\text{-}01}$ (V-PDB)') and regional records ('$\delta^{18}O_{STAL}$ (V-PDB)'): a) CANDELA (purple line), b) SIR-1 (black line), c) stacked Asiul cave records (light green line), d) ASM (green line), e) ASR (dark green line), f) LV5 (red line), g) stacked Molinos and Ejulve cave records (blue line), and h) ESP03 (orange line). The GAR-01 record is continuous, but only data overlapping with the other records is shown for clarity, resulting in apparent gaps in the GAR-01 record. Note the ASM y-axis is inverted because the r value is negative (potentially due to chronological uncertainty). In panel c, the GAR-01 record is normalised to zero to facilitate comparison with the normalised Asiul Cave record.

This approach is also consistent with the results of Daëron et al. (2019), suggesting that most Earth-surface calcites are not precipitated at equilibrium because of inherent kinetic effects occurring during deposition. If the modelled $\delta^{18}O$ ($\delta^{18}O_{mod}$) is within 0.01‰ of the actual measured $\delta^{18}O$ value for that timeslice, the simulation stops and the modelled seasonality in rainfall and temperature is recorded. The uniqueness of solutions is testable by repeatedly running the model.

### 5.2. Assumptions within the model

The model contains several assumptions. For example, the total annual rainfall amount is held constant, whereas rainfall amount undoubtedly varied interannually. This assumption is inconsequential however because rainfall seasonality drives dripwater $\delta^{18}O$ for well-buffered sites rather than the total annual rainfall; regardless, the model cannot return annual rainfall totals. At this site, the predominant control on rainfall $\delta^{18}O$ is temperature (i.e., the season in which the rain occurs) rather than the rainfall amount. This is supported by a strong relationship between monthly rainfall $\delta^{18}O$ and temperature at the Santander GNIP site ($r_s = 0.56$; $p < 0.001$; $n = 130$), however, varying moisture source region, trajectory, and moisture source $\delta^{18}O$ undoubtedly affect rainwater $\delta^{18}O$ as well. The model assumes that rainwater $\delta^{18}O$ is driven entirely by local temperature variability. Vegetation above La Garma Cave is also held constant throughout the model, whereas

in reality climatologically- and anthropogenically-driven vegetation shifts above the cave probably occurred and affected seasonal infiltration amounts (Baldini et al., 2005). Although local pollen records provide information regarding regional vegetation type through the Holocene, a localised reconstruction of vegetation density immediately above the cave has yet to be attempted, thus, this parameter is currently unquantifiable. The model includes options to parameterise soil evapotranspiration using either the Thornthwaite equation or Hamon's equation. However, the model results are optimised only when evapotranspiration is set to zero importance. 'Switching off' evapotranspiration in the model is justified based on recent empirical soil-water $\delta^{18}O$ results from La Garma Cave where evaporation was found to be negligible (Comas-Bru and McDermott, 2015). However, transpiration may play a role insofar as it can cycle moisture from the soil directly back to the atmosphere and if this is seasonal (likely for deciduous vegetation) it could impact the seasonal moisture available for infiltration to the cave. Additionally, over relatively long periods of the Holocene, vegetation changes (e.g. density, moisture use efficiency, etc.) may also have an effect. Future versions of the model may include the capability of incorporating a vegetation model pending the acquisition of new vegetation density data for the site (e.g., from local pollen reconstructions or organic markers in speleothems).

The model also assumes that the kinetic effects that are inherent to the Tremaine water-calcite fractionation factor are constant year-round; because no research has yet quantified this variability at this particular site, we are not able to incorporate this into the model. However, future versions could incorporate assumptions regarding the seasonality of disequilibrium effects (Deininger et al., 2012; Deininger and Scholz, 2019; Mühlinghaus et al., 2007) on predicted responses of the cave environment to the external climate signal, ideally by incorporating new models such as IsoCave (Guo and Zhou, 2019) or ISOLUTION (Deininger and Scholz, 2019). Research suggests that growth rate affects oxygen isotope ratios in calcite (Hansen et al., 2019; Stoll et al., 2015), although we note that these interpretations have been challenged (Dreybrodt, 2016; Dreybrodt, 2019). This first version of the model does not calculate seasonal growth rates, so it is not possible to correct for possible growth rate effects yet, although this is planned for a future version of the model. However, the observed relationship between growth rate and $\delta^{18}O$ may reflect a common control on both rather than a cause and effect relationship between growth rate and $\delta^{18}O$ (Dietzel et al., 2009; Fohlmeister et al., 2018; Gabitov et al., 2012), in which case the omission of this effect is irrelevant. Despite these assumptions, the model provides a very useful new tool for evaluating whether observed shifts in $\delta^{18}O$ records could arise from altered seasonality. The modelling results highlight time intervals when changing seasonality could have produced the observed $\delta^{18}O$ values, providing critical missing palaeoclimate information for northern Iberia and a novel method of evaluating stalagmite $\delta^{18}O$ records. However, equally informative are the intervals when the model cannot successfully converge on a value, indicating intervals when seasonality shifts are insufficient on their own to produce the stalagmite $\delta^{18}O$ values. In these few instances, another factor is necessarily implicated, highlighting intervals with considerably different boundary conditions that require a different interpretation. In theory the model could produce results on any timescale longer than annual. Here, we use 100-year long timeslices obtained by interpolating the decadally-resolved $\delta^{18}O$ data at regular 100-year intervals; the process repeated for each timeslice.

### 5.3. Modelled palaeoseasonality results

#### 5.3.1. The temperature model

The modelled monthly temperature output for the most recent timeslice matches observed monthly distribution very well, suggesting that the model is robust. The YD interval of the GAR-01 record is discussed qualitatively in Baldini et al. (2015), but here we provide quantitative estimates of seasonal temperature and rainfall (section 5.3.2. below). The YD interval within the modelled temperature data is characterised by winter temperatures that are ~7 °C lower than modern winter temperatures, and summer temperatures that are ~4 °C lower than modern summer temperatures (Fig. 8). However, our approach is limited to a maximum of 1 °C of seasonal temperature change above and beyond that suggested by the Iberian Margin SST record (Bard, 2002, 2003), so the actual temperature range may exceed this estimate. Here we do not attempt to reconstruct absolute temperatures, but instead highlight the seasonal differences in temperature and rainfall that could account for the observed $\delta^{18}O$ signal. Despite uncertainty regarding the absolute temperature range, this is consistent with a number of YD reconstructions suggesting that the event was characterised by considerably lower wintertime temperatures (Denton et al., 2005; Lie and Paasche, 2006), possibly induced by an AMOC slowdown (Lynch-Stieglitz, 2017). The recovery out of the event was rapid, and according to the GAR-01 modelling, by 9.4 ka BP monthly temperatures were slightly warmer than present day (by ~0.5 °C) (Fig. 8). The rapid amelioration in temperature at the site likely reflects the well-documented rapid deglaciation following the YD and the maximum in 60°N summer insolation centred on ~10.5 ka BP (Fig. 5) (Berger and Loutre, 1991). From the early Holocene to the date of collection, modelled temperatures gradually cool with modern winter and summer temperatures ~0.5 °C and ~0.3 °C cooler than early Holocene values. The gradual Holocene cooling, however, is punctuated by a series of warming and cooling events. Most notably, the 8.2 ka event is clearly expressed in the GAR-01 $\delta^{18}O$ record, and modelled temperatures reach a local minimum during the 8.2 ka timeslice, with winter temperatures of 10.0 °C (compared with 11.7 °C during the early Holocene). This suggests that the low $\delta^{18}O$ values observed in the GAR-01 $\delta^{18}O$ dataset resulted at least partially from cooler temperatures and increased seasonality (see section 5.3.2. below), consistent with previous results from other Atlantic margin sites (Baldini et al., 2002; Daley et al., 2016; Domínguez-Villar et al., 2009). This is the lowest winter temperature modelled for the early Holocene, and in fact only at 4.3 ka BP do winter temperatures drop below the 8.2 ka values, reaching as low as 9.5 °C, potentially reflecting the well-documented '4.2 ka event' (Fig. 8). The expression of the '4.2 ka event' in the $\delta^{18}O$ data is rather muted, although it does appear in the Smith et al. (2016) record from nearby Asiul Cave. The event may have contributed to severe Middle East drought affecting civilisations at the time (Cullen et al., 2000; Hsiang et al., 2013). The expression of the event as one of the coolest timeslices of the Holocene, combined with its presence in other north Iberian records, suggests that the 4.2 ka event did affect the western margin of Europe as well as the Middle East. This is discussed in more depth below.

Modelled GAR-01 temperature variability is of a very similar amplitude as the Martin-Chivelet et al. (2011) temperature reconstruction over the last 4 ka (Fig. 8), with several key features duplicated. For example, both records suggest substantial centennial-scale temperature variability from 4 to 2.5 ka BP, and exhibit a pronounced warming event at ~3 ka BP. A very pronounced warming event in the Mary et al. (2017) Bay of Biscay SST record at ~2 ka BP is not reproduced either in the GAR-01 modelled temperature record or in the Martin-Chivelet et al. (2011) temperature reconstruction, suggesting that this temperature anomaly was largely restricted to the marine environment and only briefly affected terrestrial Iberian temperatures. Modelled GAR-01 temperatures show a maximum value at 1 ka BP, consistent with both

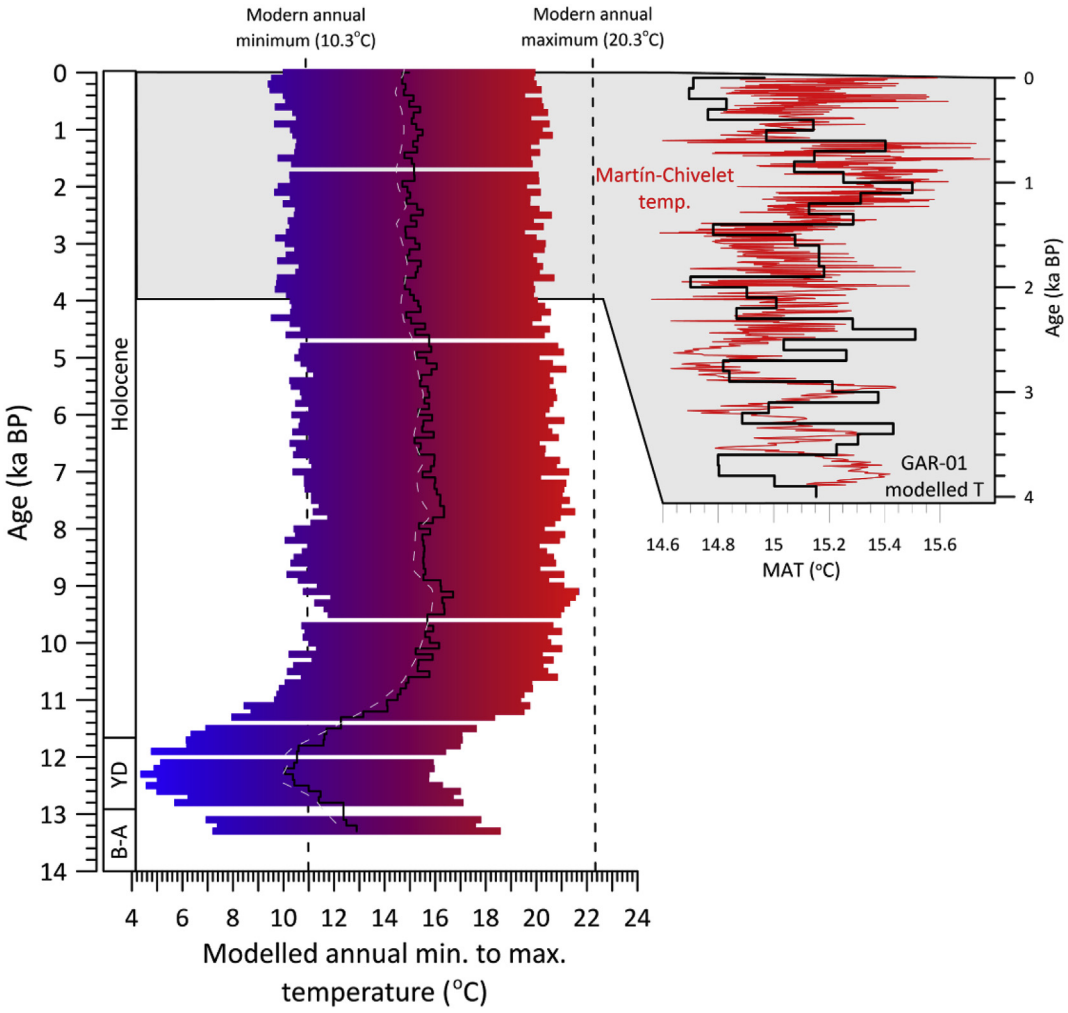


**Fig. 8.** The modelled outside air temperature range above La Garma Cave through the Holocene and the YD in 100-year timeslices. The two vertical black dashed lines illustrate the mean modern February (10.3 °C) and July (20.3 °C) temperatures at the Santander GNIP station over the interval from 2000 to 2010. The Mean Annual Temperature (MAT) is plotted as a black step-plot together with the Iberian SST record from Bard (2002) (dashed white line). The offset between MAT at the La Garma site and Iberian Margin SST record site is corrected for using the most recent value in the Iberian Margin record, and this offset is applied throughout the rest of the study interval; this produces the slight apparent offset between the two records through the Holocene. The inset shows the modelled GAR-01 MAT and a temperature reconstruction for northern Iberia based on stalagmite $\delta^{13}C$ values (Martin-Chivelet et al., 2011), while the black crosses show a recent alkenone-derived SST record from offshore SW Iberia for comparison (SHAK06–5 K at 37°34N, 10°09W) (Ausin et al., 2019). Both the Martin-Chivelet and Ausin records are independent of the modelling, and have not been rescaled, so regional temperature differences remain.

the Martin-Chivelet et al. (2011) temperature reconstruction for northern Iberia (Fig. 8) and a comprehensive review of Iberian terrestrial climate proxy evidence (Moreno et al., 2012), and was probably linked to the Medieval Climate Anomaly (MCA). Over the most recent millennium, modelled GAR-01 temperatures suggest that minimum temperatures associated with the Little Ice Age (LIA) occurred from 1700 to the 1800 s C.E., rather than ~300 years earlier as suggested by the Martin-Chivelet et al. (2011) temperature reconstruction. The modelled temperature values are however consistent with the most substantial advance in mountain glaciers across Iberia during the late LIA (Trueba et al., 2008), as well as extensive periglacial landforms dated to between 1700 and 1900 C.E. (Oliva et al., 2016, 2018). The modelled temperature output therefore appears to accurately reflect known temperature fluctuations during the last two millennia, capturing both LIA cooling and MCA warming. Overall, the excellent agreement between the modelled temperature output and existing temperature reconstructions over the last 4 ka BP strongly suggest that the modelling approach is reasonable, supporting interpretations over the older less-well constrained intervals of the record.

*5.3.2. The rainfall model*

The model run for the most recent timeslice (from 2000 to 1900 C.E., or −0.050 to 0.050 ka BP) converges on an annual distribution of rainfall which matches current observed seasonality (Figs. 9 and 10a), supporting the modelling approach. The model suggests that the seasonal rainfall pattern in northern Iberia had a modern polarity (i.e., rainier winters, drier summers) for 71% of the Holocene. Several intervals of reversed polarity (i.e., the opposite of present day) seasonal rainfall are also present (Fig. 9), and the model helps ground-truth interpretations based on the $\delta^{18}O$ datasets. One of the most notable intervals of reversed polarity seasonal rainfall occurs during the 12.80 ka BP timeslice, during the early YD (Fig. 10f). The modelled results suggest that peak rainfall at 12.80 ka BP occurred during the summer (~115 mm in August) whereas the driest month was November with ~65 mm of rainfall (Fig. 10f). A very low GAR-01 $\delta^{18}O$ value exists at this date, which was interpreted by Baldini et al. (2015) as reflecting cold conditions consistent with an AMOC slowdown and increased sea ice across the North Atlantic. As discussed above (section 5.2.1.), the model supports this interpretation, but here we can add additional detail. If modern rainfall

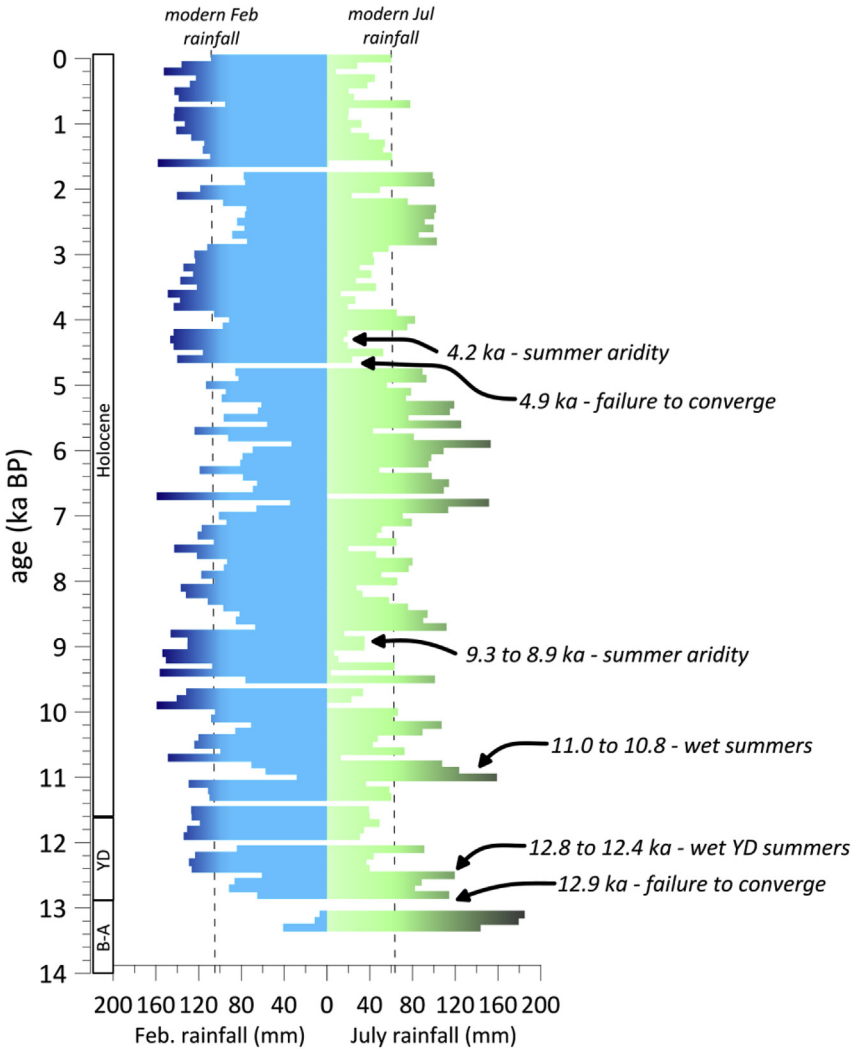


**Fig. 9.** The modelled range in rainfall in 100-year timeslices over the length of the GAR-01 record, where the bar on the left indicates modelled November rainfall (currently the month with the highest rainfall in the Santander rainfall record) and the bar on the right indicates modelled July rainfall (currently the month with the lowest rainfall in the Santander rainfall record). Intervals where the modelled $\delta^{18}O$ fails to converge on the actual $\delta^{18}O$ have no bars. The vertical dashed lines show the current rainfall amount for July and November (49.5 mm and 118.8 mm, respectively). In all cases, the total annual rainfall is held constant (consequently, the length of the bar for every timeslice is identical). The darker shading in both summer and winter indicates timeslices when rainfall totals are higher than current values.

polarity were extant during the early YD, considerably lower $\delta^{18}O$ values would have resulted via the considerably colder winter temperatures characteristic of that interval combined with high winter rainfall. The $\delta^{18}O$ minimum at 12.80 ka BP is therefore the result of low temperatures combined with decreased winter rain and higher summer rainfall, which combined to moderate the early YD $\delta^{18}O$ decrease. Increased distance from the coast during the YD due to the low sea level associated with the last glacial may have contributed to lowering the $\delta^{18}O$ somewhat, but because sea level did not drop into the YD, this is probably not the main driver. Moreover, the distance to the coast was never much greater than today, as Cantabria's continental shelf is quite narrow. Interestingly, this result suggests that the presence of similarly low $\delta^{18}O$ values during the YD, Greenlandian, and Northgrippian (Fig. 5) partially stems from higher than expected $\delta^{18}O$ values during the YD rather than particularly low values during the other intervals.

In contrast, by 9.4 ka BP temperatures were high (about 0.5 °C higher than modern values), and the model suggests that summer rainfall was essentially non-existent (Figs. 9 and 10d). An alternative is that summer rainfall did occur, but substantial amounts of summer evapotranspiration eliminated most summer recharge. However, this is not supported by the modelling results, where the incorporation of evapotranspiration reduces the ability of the model to converge onto a solution. This summer aridity suggests that a Mediterranean-like climate may have existed in northern Iberia at this time, consistent with a northward displaced Azores High that may have accompanied increasing insolation (Fig. 11). This is also consistent with the interpretations of Walczak et al. (2015) who argued that increased year-round moisture in southern Iberian was triggered by a northward displaced Azores High. The westerly storm track would have also shifted to the north, and indeed records suggest increased moisture delivery to Scandinavia (Bakke et al., 2009) and reduced moisture to southern France (Genty et al., 2006; Wirth et al., 2013) and northern Iberia (Aranbarri et al., 2014; Railsback et al., 2011) at this time. During the 8.2 ka event, winters appear wetter than at present day, but numerous other intervals also exist across the Holocene with similar amounts of winter rainfall. The model suggests that rainfall was strongly biased towards the summer over a 2 kyr period from ~7 to ~5 ka BP (Fig. 11). For example, at 5.9 ka BP, July rainfall was

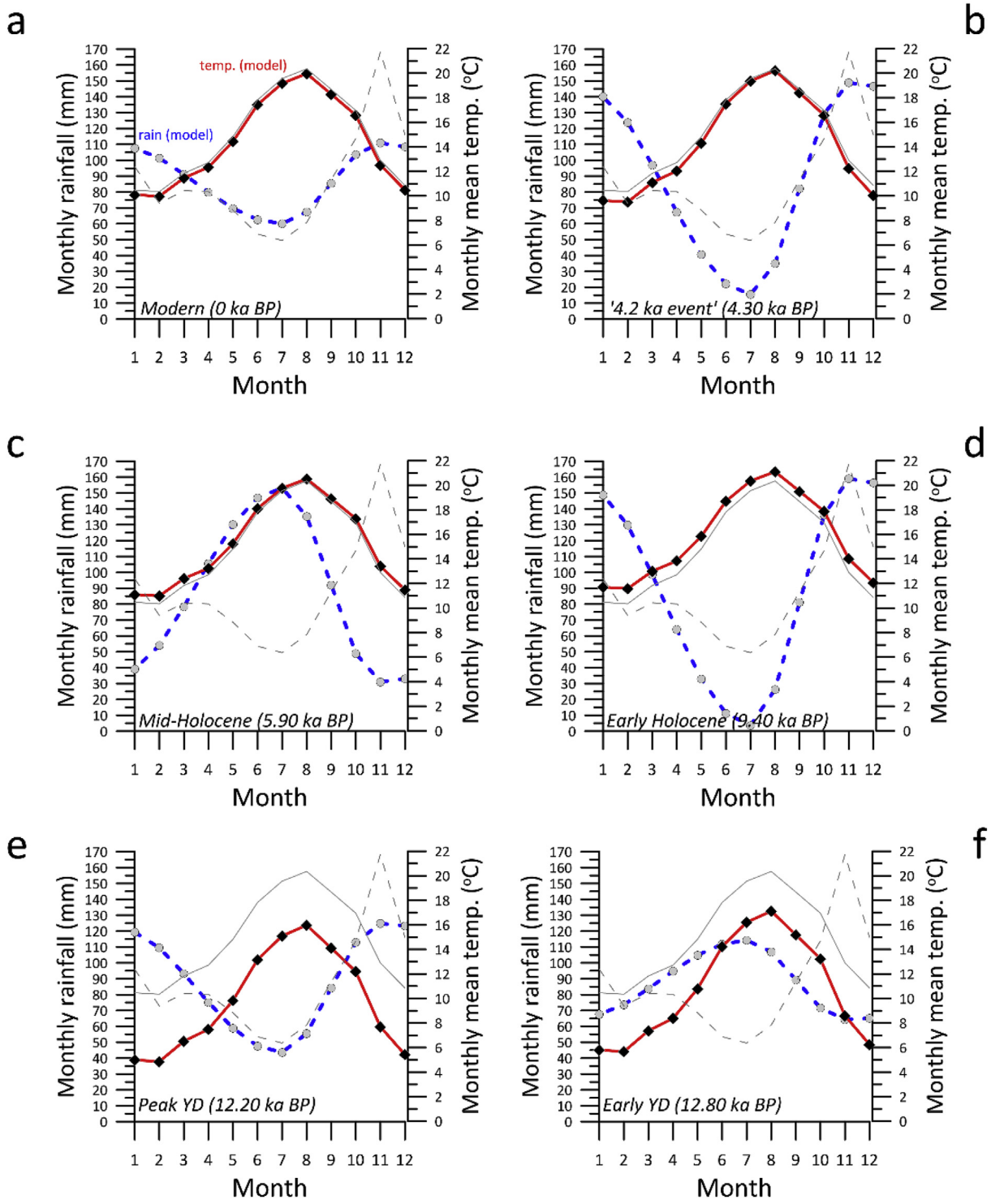


**Fig. 10.** Selected 100-year timeslices of seasonality modelled using the GAR-01 record as an input. In each panel, the current seasonal distribution in temperature and rainfall at the Santander GNIP site are shown (solid and dashed grey lines, respectively), as well as timeslice-specific temperature (solid red line with diamonds) and rainfall (dashed blue line with circles) outputs. Shown are 100-year timeslices centred on a) 0 ka BP, b) 4.30 ka BP, c) 5.90 ka BP, d) 9.40 ka BP, d) 12.20 ka BP, and e) 12.80 ka BP.

153 mm compared to the modelled November total of just 31 mm (Fig. 10c). The end of this mid-Holocene interval of reversed polarity rainfall seasonality coincides with the establishment of Mediterranean conditions in southern Iberia at 5.3 ka BP, as well as the shift from a mostly positive NAO to a more negative NAO (Olsen et al., 2012). Both of these phenomena are likely due to southward displacement of the Azores High following the Holocene thermal maximum, consistent with elevated summer rainfall at 5.9 ka BP in northern Iberia slowly giving way to drier summers by ~4.8 ka BP (Fig. 9). According to the rainfall model output (Figs. 9 and 10b), very low $\delta^{18}O$ values at 4.2 ka BP are the result of the development of very arid summers (combined with cooler temperatures), the

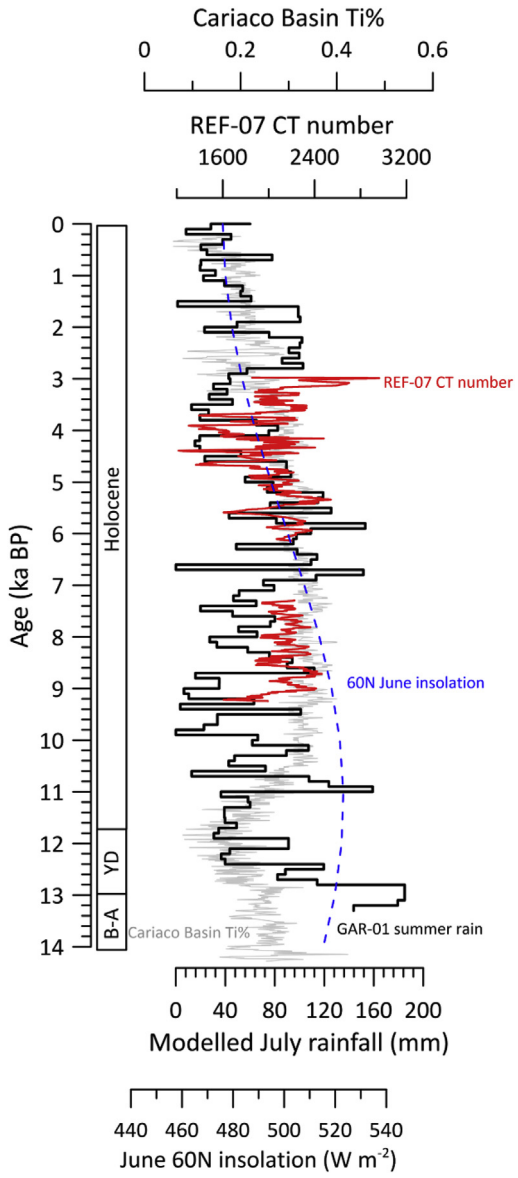


**Fig. 11.** Modelled summer rainfall totals derived from the GAR-01 $\delta^{18}O$ record (black) compared with proxies for the ITCZ (the Cariaco Basin Ti% record (light grey) (Haug et al., 2001) with the revised chronology of Kennett et al. (2012)) and the Azores High (the REF-07 stalagmite density record from El Refugio Cave, southern Iberia (red) (Walczak et al., 2015). Also shown is June insolation at 60°N (blue) (Berger and Loutre, 1991).

culmination of a summer drying trend starting at peak summer rainfall during the mid-Holocene; this biases the annual recharge towards low $\delta^{18}O$ winter rainfall. The well-documented '4.2 ka event' is linked to a reduction in Northern Hemisphere monsoonal system strength (Booth et al., 2005; Staubwasser et al., 2003) and is implicated in dramatic cultural change at several locations (deMenocal, 2001; Stanley et al., 2003), but particularly in the Middle East (Arz et al., 2017; Drysdale et al., 2006; Staubwasser et al., 2003). The event coincides with a peak in North Atlantic ice rafted debris possibly induced by solar variability (Bond et al., 2001). However, in our modelled rainfall seasonality dataset and in the $\delta^{18}O$ data, the 4.2 event summer aridity is the culmination of a longer summer drying trend starting after peak mid-Holocene summer rainfall at 5.9 ka BP (Fig. 9). This perspective is consistent with data from an Italian flowstone record also suggesting that the 4.2 ka event occurred near the end of a longer drying trend and that it may have a different origin than other Holocene drying events (Drysdale et al., 2006). Another interval of higher summer rainfall occurs from ~2.8 to ~1.8 ka BP, but rainfall occurs in the winter as well (although slightly reduced compared to modern values). From 1.6 ka BP to present day the rainfall distribution has a modern polarity, with the LIA characterised by enhanced seasonality with drier than modern summers. The rainfall and temperature distribution of the LIA is very similar to that observed in the model output during the 4.2 ka event, perhaps indicative of a similar origin.

### 5.3.3. LA-ICPMS analysis of the 4.2 ka event

Monthly-scale LA-ICPMS trace element data were obtained across the interval containing the 4.2 ka event, from 3.79 to 4.98 ka BP (Fig. 12). These data permit not only the reconstruction of climate with excellent detail, but also help corroborate the results of the seasonality model discussed above. Unfortunately determining the polarity of the seasonality is not possible, but the amplitude of any seasonality present is assessable.

Mg concentrations in GAR-01 were previously interpreted as reflecting seaspray contribution. Mg and Sr data over the 4.2 ka event in GAR-01 are consistent with this interpretation and an approximate marine aerosol contribution to drip water and, ultimately to GAR-01 calcite, of 2% (Fig. S4). Thus, aerosol-derived Mg concentrations decrease gradually from a peak at ~5.0 ka BP until 4.2 ka BP, interrupted by several large Mg excursions (including at 4.9 ka BP) (Fig. 12a). This may reflect the decreasing influence of seaspray, following on from the interpretations of Baldini et al. (2015) for the YD interval within the same stalagmite. The mid-Holocene interval analysed containing the 4.2 ka event generally has considerably less Mg (545 ppm) than the mean value for the YD interval (843 ppm), potentially reflecting weaker winds and less seaspray affecting the coastal La Garma Cave site during the mid-Holocene than during the YD. Another possible factor is a shift in the direction of predominant winds due to a shifted Azores High, leading to a reduction of winds coming off the sea and consequently in seaspray. The model suggests pronounced summer aridity in northern Iberia between 4.2 and 4.5 ka BP, coincident with the lowest Mg values of the interval (<300 ppm). The mechanisms through which summer aridity might produce low Mg concentrations in GAR-01 include: i) reduced seaspray contributions due to a generally amenable climate and calm winds, even in winter, ii) very low Mg during winter due to high winter rainfall, or iii) a combination of i and ii.

During the YD interval, seasonality is generally not apparent in the Mg data (Fig. 12e), almost certainly reflecting low growth rates across this interval, where even the high-resolution LA-ICPMS data cannot tease out annual cycles. The growth rate during the YD interval is estimated at ~25 μm $year^{-1}$ and the LA-ICPMS data were obtained at a ~15 μm effective resolution; consequently discerning an annual cycle is not possible. The mean Mg concentration values are considerably higher than the Holocene values, interpreted as reflecting more winter storms, stronger winds, and higher seaspray contributions to rainwater (Baldini et al., 2015). A similar lack of seasonality is apparent at ~4.8 ka BP (Fig. 12d), but the U-Th chronology suggests that the growth rate was sufficiently rapid to permit the detection of an annual cycle. This probably reflects year-to-year growth rate changes that are not apparent in the U-Th chronology, and that the interval around 4.8 ka BP reflects slower growth than that implied by the relatively low-resolution U-Th chronology. The evolution to gradually more well-developed annual cycles from ~4.8 ka BP to ~4.2 ka BP (Fig. 12 b-d) potentially reflects steadily increasing growth rates at time-scales not easily discernible using U-Th dating. We therefore suggest that

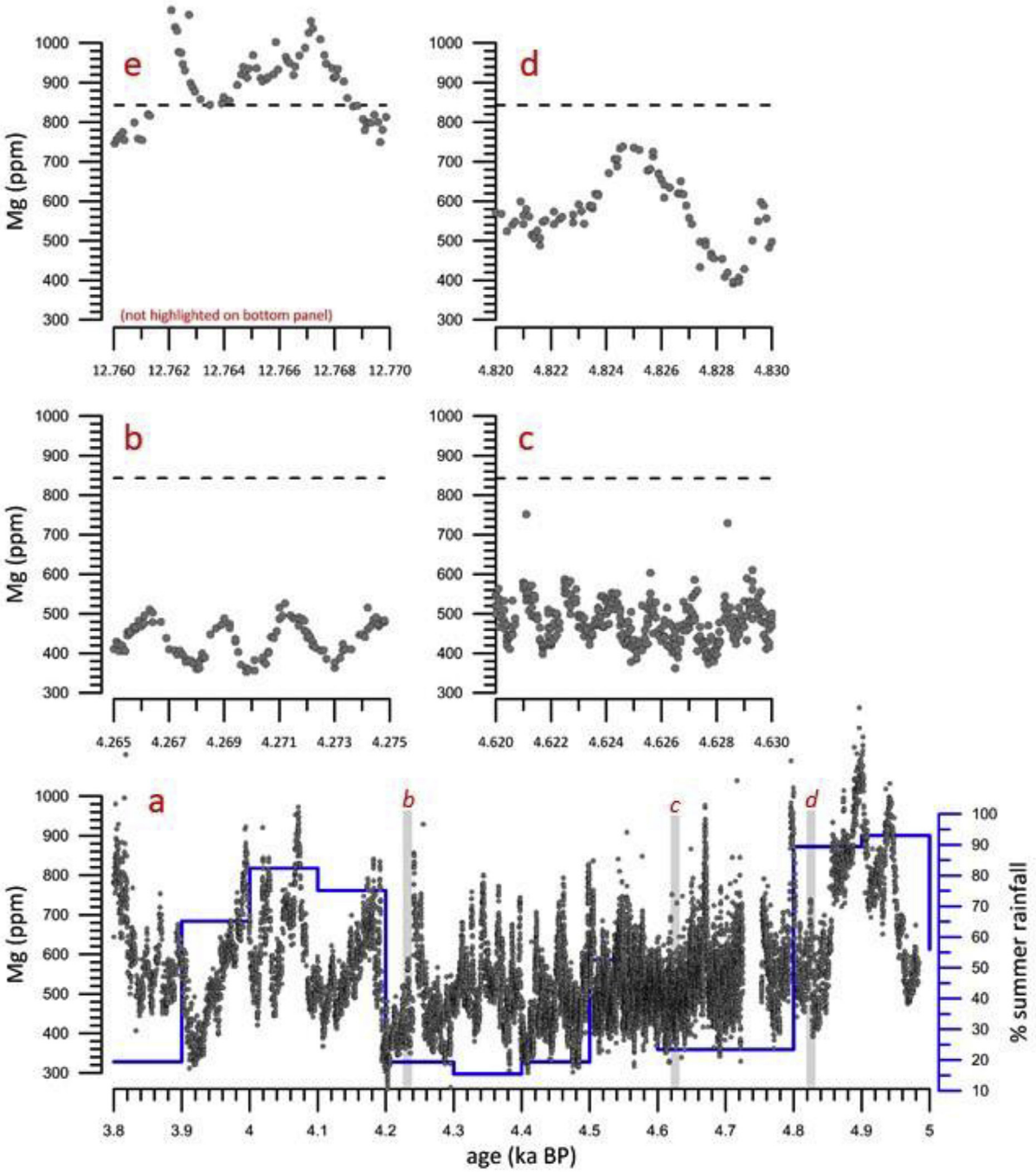


**Fig. 12.** High-resolution (monthly-scale) LA-ICPMS Mg concentration data across the 4.2 ka event (panel a) and for selected 10-year windows (panels b–e) during the interval 4.830 to 4.265 ka BP (b–d) and the YD (e). The model derived % summer rainfall is also shown in (a) (blue line). Note that panel e illustrates a 10-year period during the Younger Dryas interval discussed in Baldini et al. (2015) for comparison with the select mid-Holocene data. The longer YD record is not shown here; see Baldini et al. (2015). Panels c–e have identically scaled x- and y-axes and the horizontal dashed line in each panel represents the mean Mg concentration across the entire YD event (11.7–12.880 ka BP) rather than just the 10-year window shown in (e). Vertical grey bars in panel (a) labelled *b*, *c*, and *d* provide the relative timing of the 10-year windows presented in panels b, c, and d, respectively.

climate leading up to the 4.2 ka event in north Iberia was characterised by gradually decreasing summer rainfall (the increasing bias towards winter rainfall producing lower $\delta^{18}O_{cal}$ values), steadily increasing total annual rainfall (contributing to lower $\delta^{18}O$ and lower Mg values), and a steady increase in GAR-01 growth rates (evident through progressively more clearly expressed annual cycles).

In northern Iberia, we propose that the 4.2 ka BP event was characterised by Mediterranean-like climate conditions that promoted rapid stalagmite growth (e.g., rapid growth is characteristic of stalagmites from Mediterranean-influenced sites like El Refugio cave (Fig. 1) (Walczak et al., 2015). Similar conditions also existed in the early Holocene, and we suggest that both reflect the summertime influence of the Azores High. The early Holocene pseudo-Mediterranean climate was caused by the insolation-controlled northward migration of the Azores High (Fig. 11), whereas the

climate leading into the 4.2 ka event was caused by the slow migration of the Azores High due to south tracking decreasing insolation. This interpretation is also consistent with observed Northern Hemisphere monsoonal weakening and southward ITCZ migration over the Holocene (Haug et al., 2001) (Fig. 11). The GAR-01 Mg concentration data (Fig. 12) do not contain any evidence for a discrete, short-lived 4.2 ka event; rather the 'event' was the culmination of a ~1000-year period of slowly changing climate. The interval including and leading into the 4.2 ka event represents the last prolonged episode of very 'anomalous' climate prior to the emplacement of an essentially modern climate system in northern Iberia.

## 6. Conclusions

The GAR-01 $\delta^{18}O$ record provides the first continuous stalagmite record from northern Iberia covering both the Holocene and the Younger Dryas, permitting replication of shorter and/or discontinuous records across this interval. All the published northern Iberian $\delta^{18}O$ records correlate reasonably well with the GAR-01 $\delta^{18}O$ record in terms of the nature of the variability observed, suggesting that all the records are robust and affected by essentially the same factors. Differences probably reflect the low signal-to-noise ratio of the data across the Holocene combined with dating uncertainty, or cave-specific factors. The 8.2 ka event is clearly expressed in the GAR-01 record with a similar double-pronged expression as in the nearby Kaite Cave record (Domínguez-Villar et al., 2009, 2017). Growth hiatuses (e.g., Asiul Cave – ASR; El Soplao Cave – SIR-1) and erosional surfaces (e.g., Cova da Arcoia - ESP03) across the event are common in regional records. The presence of a $\delta^{18}O$ anomaly in both the Kaite and La Garma Cave records, and the interruptions in stalagmite growth associated with the 8.2 ka event in other records, suggests that the event affected climate across northern Iberia.

A single climate variable (e.g., temperature, rainfall amount, etc.) cannot explain many features of the GAR-01 $\delta^{18}O$ record, indicating that the climate signal in northern Iberia was complex. In particular, three intervals exist when GAR-01 $\delta^{18}O$ was particularly low (−5.00 at 4.709 ka BP; −5.08‰ at 8.974 ka BP; −5.01‰, at 12.290 ka BP). These values occurred during both cold (the YD) and warm intervals (the early and mid-Holocene), precluding temperature change as the dominant control on $\delta^{18}O$ through the entirety of the record.

Herein, the effects of variable seasonality on the GAR-01 $\delta^{18}O$ record was investigated using a simple Monte Carlo model, which randomly altered the seasonal rainfall and temperature distribution for individual 100-year time slices until the modelled $\delta^{18}O_{mod}$ results matched the measured $\delta^{18}O$ values for that timeslice. The results suggest that seasonal rainfall and temperature distribution variability can successfully account for 95% of the record. Only seven timeslices exist where the model does not converge, suggesting the influence of a factor not considered in the model. Interestingly, two of these timeslices are at 13.0 and 12.9 ka BP, coinciding with the YD event's initiation, and may represent poorly understood large-scale atmospheric and oceanic re-organisation associated with this event. The other intervals where the model fails to converge are at 12, 11.4, 9.6, 4.7, and 1.7 ka BP. The modelled seasonality reconstruction can therefore account for the vast majority of the observed $\delta^{18}O$ variability, and presents a ~13 ka BP model of seasonal temperature and rainfall shifts in northern Iberia.

The model suggests that the low $\delta^{18}O$ values occurring during the peak YD were primarily the result of low regional air temperatures, consistent with Baldini et al. (2015), but provides new insights into climate seasonality during the event. The model results suggest that the YD was characterised by cold, dry winters and cool, wet summers. Interestingly, this interval of reversed polarity conditions (compared to modern) resulted in $\delta^{18}O$ values that, although low, were higher than if rainfall (or snowfall) had occurred predominantly in the winter. This interpretation is consistent with a variety of research suggesting that the YD was characterised by considerably colder winter but only marginally cooler summer temperatures (Denton et al., 2005); the extreme winter cooling would have also reduced evaporation from the North Atlantic and consequently rainfall during the winter. Extensive winter sea ice across the North Atlantic during very cold YD winters would also have reduced moisture uptake from the sea surface. The presence of equivalent low $\delta^{18}O$ values in the GAR-01 record in both YD and mid-Holocene timeslices is therefore explicable partially by higher than expected values during the YD.

Climate in northern Iberia during the early Holocene was affected by a northward shifted Azores High that produced extremely arid summers but sustained winter rainfall. The presence of a Mediterranean-like climate in northern Iberia is consistent with other Iberian and European records tracking both the Azores High and the position of associated westerly winds (e.g., Walczak et al., 2015; Bakke et al., 2009; Wirth et al., 2013). Mid-Holocene climate was similarly dominated by the position and strength of the Azores High as it slowly migrated to the south, tracking insolation. From ~7 to ~5 ka BP rainfall was strongly biased towards the summer, and the end of this reversed polarity rainfall seasonality interval coincided with the establishment of Mediterranean conditions in southern Iberia at 5.3 ka BP, as well as the shift from a mostly positive NAO to a more negative NAO shortly afterwards (from 5.2 to 4.4 ka BP) (Olsen et al., 2012), again probably due to southward displacement of the Azores High. The model suggests that summers were becoming drier by ~4.8 ka BP, a trend culminating in very arid summers at ~4.2 ka BP. The lack of summer rainfall and abundant low $\delta^{18}O$ winter rainfall would have biased annually averaged recharge, which is well-integrated at the La Garma Cave site, towards winter rainfall values, consequently explaining the low $\delta^{18}O$ values observed during this time interval. This peak in summer aridity is probably associated with the globally-observed 4.2 ka event (Booth et al., 2005; Staubwasser et al., 2003). In GAR-01, the event appears as the peak of the summer drying trend that lasted almost 1 kyr, consistent with flowstone data from Italy (Drysdale et al., 2006). This interpretation is supported by a high-resolution LA-ICPMS transect of the 4.2 ka event interval, and we suggest that the 4.2 ka event in northern Iberia was characterised by higher than average annual mean rainfall with very arid summers. A modern polarity in rainfall is achieved at 1.6 ka BP and persists until the present day; the rainfall distribution during the LIA was characterised by a slightly amplified modern rainfall polarity, with drier than modern summers.

We stress however that these modelling results represent one possible scenario, and the geochemical data is potentially explicable by appealing to other mechanisms, such as shifts in moisture mass trajectory, moisture source region, or evapotranspiration regime not detected by the model. Regardless, seasonality shifts are among the most parsimonious explanations for the observed variability during the climatologically subdued Holocene, a conclusion supported by a recent comprehensive review of Iberian climate suggesting that seasonality is a key variable over the Holocene (Moreno et al., 2017). This study therefore presents critical missing information bridging the Holocene and the Pleistocene in a climatologically sensitive region affected by both AMOC and the NAO.

The modelling approach discussed here provides a more detailed view of climate change compared to a semi-quantitative discussion of the $\delta^{18}O$ record in isolation. Although rainfall amount certainly varied from year-to-year across the last 13 ka, the

model suggests that seasonality shifts can explain the vast majority of the GAR-01 $\delta^{18}O$ record's variability. This approach potentially provides critical missing seasonality data for northern Iberia and is supported by high resolution trace element data across the 4.2 ka and Younger Dryas events, but other monthly-scale records are needed to confirm the model's output across other intervals. The same modelling approach is also tenable for $\delta^{18}O$ records from other sites and may help highlight aspects of any record that are explicable by appealing to seasonality shifts. Intervals where a model does not converge could highlight climate anomalies forced by unusual factors. Future stalagmite-based palaeoclimate research could benefit from using similar approaches to support interpretations based on geochemical climate proxies alone.

## Acknowledgements

This research was funded by FMcD's Enterprise Ireland Basic Research Grants Scheme and conducted in parallel with IJF's Natural Environment Research Council (NERC) RAPID climate change programme funded ASCRIBE Project (Grant NER/T/S/2002/00448). FMcD acknowledges support from Science Foundation Ireland through Research Frontiers Grants 07/RFP/GEOF265 and 08/FRP/GEO1184. The Archaeological work at La Garma has been funded by the Consejería de Educación, Cultura y Deporte del Gobierno de Cantabria. We thank Jens Fohlmeister and two anonymous reviewers for their helpful comments which improved the manuscript. We also thank Ana Moreno for her editorial inputs and useful comments that similarly improved the manuscript.

## Appendix A. Supplementary data

Supplementary data to this article can be found online at https://doi.org/10.1016/j.quascirev.2019.105998.

## References

Aranbarri, J., Gonzalez-Samperiz, P., Valero-Garces, B., Moreno, A., Gil-Romera, G., Sevilla-Callejo, M., Garcia-Prieto, E., Di Rita, F., Mata, M.P., Morellon, M., Magri, D., Rodriguez-Lazaro, J., Carrion, J.S., 2014. Rapid climatic changes and resilient vegetation during the Lateglacial and Holocene in a continental region of south-western Europe. Glob. Planet. Chang. 114, 50–65.

Arias, P., 2009. Rites in the dark? an evaluation of the current evidence for ritual areas at Magdalenian cave sites. World Archaeol. 41, 262–294.

Arias, P., Laval, E., Menu, M., Sainz, C.G., Ontanon, R., 2011. Pigments in parietal and portable upper Palaeolithic art of La Garma(Cantabria, Spain). Anthropologie 115, 425–445.

Arias, P., Ontañón, R., 2012. La Garma (Spain): long-term human activity in a karst system. In: Skeates, K.A.B.a.R. (Ed.), Caves in Context. The Cultural Significance of Caves and Rockshelters in Europe. Oxbow, Oxford, pp. 101–117.

Arias, P., Sainz, C.G., Romanillo, A.M., Peredo, R.O., 2001. La Garma: Un Descenso Al Pasado. Cosejeria de Cultura y Deporte del Gobierno de Cantabria y Universidad de Cantabria, Santander, p. 109.

Arz, H.W., Lamy, F., Pätzold, J., 2017. A pronounced dry event recorded around 4.2 ka in brine sediments from the northern red sea. Quat. Res. 66, 432–441.

Ausin, B., Haghipour, N., Wacker, L., Voelker, A.H.L., Hodell, D., Magill, C., Looser, N., Bernasconi, S.M., Eglinton, T.I., 2019. Radiocarbon age offsets between two surface Dawelling planktonic foraminifera species during abrupt climate events in the SW Iberian margin. Paleoceanogr. Paleocl. 34, 63–78.

Baker, A., Hartmann, A., Duan, W.H., Hankin, S., Comas-Bru, L., Cuthbert, M.O., Treble, P.C., Banner, J., Genty, D., Baldini, L.M., Bartolome, M., Moreno, A., Perez-Mejias, C., Werner, M., 2019. Global analysis reveals climatic controls on the oxygen isotope composition of cave drip water. Nat. Commun. 10.

Baker, A., Hellstrom, J.C., Kelly, B.F.J., Mariethoz, G., Trouet, V., 2015. A composite annual-resolution stalagmite record of North Atlantic climate over the last three millennia. Sci. Rep. 5.

Bakke, J., Lie, O., Heegaard, E., Dokken, T., Haug, G.H., Birks, H.H., Dulski, P., Nilsen, T., 2009. Rapid oceanic and atmospheric changes during the Younger Dryas cold period. Nat. Geosci. 2, 202–205.

Baldini, J.U.L., McDermott, F., Baker, A., Baldini, L.M., Mattey, D.P., Railsback, L.B., 2005. Biomass effects on stalagmite growth and isotope ratios: a 20th century analogue from Wiltshire, England. Earth Planet. Sci. Lett. 240, 486–494.

Baldini, J.U.L., McDermott, F., Fairchild, I.J., 2002. Structure of the 8200-year cold event revealed by a speleothem trace element record. Science 296, 2203–2206.

Baldini, J.U.L., McDermott, F., Fairchild, I.J., 2006. Spatial variability in cave drip water hydrochemistry: implications for stalagmite paleoclimate records. Chem. Geol. 235, 390–404.

Baldini, L.M., McDermott, F., Baldini, J.U.L., Arias, P., Cueto, M., Fairchild, I.J., Hoffmann, D.L., Mattey, D.P., Muller, W., Nita, D.C., Ontanon, R., Garcia-Monco, C., Richards, D., 2015. Regional temperature, atmospheric circulation, and sea-ice variability within the Younger Dryas Event constrained using a speleothem from northern Iberia. Earth Planet. Sci. Lett. 419, 101–110.

Baldini, L.M., McDermott, F., Foley, A.M., Baldini, J.U.L., 2008. Spatial variability in the European winter precipitation $\delta^{18}$ O-NAO relationship: implications for reconstructing NAO-mode climate variability in the Holocene. Geophys. Res. Lett. 35, L04709.

Bard, É., 2002. Abrupt climate changes over millennial time scales: climate shock. Phys. Today 55, 32–38.

Bard, É., 2003. North-Atlantic sea surface temperature reconstruction. In: Paleoclimatology IPWDCf (Ed.), Data Contribution Series #2003-026. NOAA/NGDC Paleoclimatology Program, Boulder CO, USA.

Berger, A., Loutre, M.F., 1991. Insolation values for the climate of the last 10000000 years. Quat. Sci. Rev. 10, 297–317.

Bond, G., Kromer, B., Beer, J., Muscheler, R., Evans, M.N., Showers, W., Hoffmann, S., Lotti-Bond, R., Hajdas, I., Bonani, G., 2001. Persistent solar influence on north Atlantic climate during the Holocene. Science 294, 2130–2136.

Bond, G., Showers, W., Cheseby, M., Lotti, R., Almasi, P., deMenocal, P., Priore, P., Cullen, H., Hajdas, I., Bonani, G., 1997. A pervasive millennial-scale cycle in North Atlantic Holocene and glacial climates. Science 278, 1257–1266.

Bond, G., Showers, W., Elliot, M., Evans, M., Lotti, R., Hajdas, I., Bonani, G., Johnsen, S., 1999. The North Atlantic's 1-2 Kyr Climate Rhythm: Relation to Heinrich Events, Dansgaard/Oeschger Cycles and the Little Ice Age, Mechanisms of Global Cliamte Change at Millenial Time Scales. American Geophysical Union, pp. 35–58.

Booth, R.K., Jackson, S.T., Forman, S.L., Kutzbach, J.E., Bettis, E.A., Kreig, J., Wright, D.K., 2005. A severe centennial-scale drought in mid-continental North America 4200 years ago and apparent global linkages. Holocene 15, 321–328.

Bourges, F., Mangin, A., d'Hulst, D., 2001. Le gaz carbonique dans la dynamique de l'atmosphère des cavités karstique: l'exemple de l'Aven d'Orgnac (Ardèche). Earth Planet. Sci. 333, 685–692.

Breitenbach, S.F.M., Rehfeld, K., Goswami, B., Baldini, J.U.L., Ridley, H.E., Kennett, D.J., Prufer, K.M., Aquino, V.V., Asmerom, Y., Polyak, V.J., Cheng, H., Kurths, J., Marwan, N., 2012. COnstructing proxy records from age models (COPRA). Clim. Past 8, 1765–1779.

Carolin, S.A., Walker, R.T., Day, C.C., Ersek, V., Sloan, R.A., Dee, M.W., Talebian, M., Henderson, G.M., 2019. Precise timing of abrupt increase in dust activity in the Middle East coincident with 4.2 ka social change. Proc. Natl. Acad. Sci. U.S.A. 116, 67–72.

Cheng, H., Edwards, R.L., Hoff, J., Gallup, C.D., Richards, D.A., Asmerom, Y., 2000. The half-lives of uranium-234 and thorium-230. Chem. Geol. 169, 17–33.

Cohen, K.M., Finney, S.C., Gibbard, P.I., Fan, J.-X., 2013. The ICS international chronostratigraphic chart. Episodes 36, 199–204.

Comas-Bru, L., McDermott, F., 2014. Impacts of the EA and SCA patterns on the European twentieth century NAO-winter climate relationship. Q. J. Roy. Meterol. Soc. 140, 354–363.

Comas-Bru, L., McDermott, F., 2015. Data-model comparison of soil–water δ18O at a temperate site in N. Spain with implications for interpreting speleothem δ18O. J. Hydrol. 530, 216–224.

Coplen, T.B., 2007. Calibration of the calcite-water oxygen-isotope geothermometer at Devils Hole, Nevada, a natural laboratory. Geochem. Cosmochim. Acta 71, 3948–3957.

Cullen, H.M., deMenocal, P.B., Hemming, S., Hemming, G., Brown, F.H., Guilderson, T., Sirocko, F., 2000. Climate change and the collapse of the Akkadian empire: evidence from the deep sea. Or. Geol. 28, 379–382.

Daëron, M., Drysdale, R.N., Peral, M., Huyghe, D., Blamart, D., Coplen, T.B., Lartaud, F., Zanchetta, G., 2019. Most Earth-surface calcites precipitate out of isotopic equilibrium. Nat. Commun. 10.

Daley, T.J., Barber, K.E., Hughes, P.D.M., Loader, N.J., Leuenberger, M., Street-Perrott, F.A., 2016. The 8.2-ka BP event in north-eastern North America: first combined oxygen and hydrogen isotopic data from peat in Newfoundland. J. Quat. Sci. 31, 416–425.

de Oliveira, A.C., da Silva Lima, A., 2010. Spatial variability in the stable isotopes of modern precipitation in the northwest of Iberia. Isotopes Environ. Health Stud. 46 (1), 13–26. https://doi.org/10.1080/10256010903388154.

Deininger, M., Fohlmeister, J., Scholz, D., Mangini, A., 2012. Isotope disequilibrium effects: the influence of evaporation and ventilation effects on the carbon and oxygen isotope composition of speleothems - a model approach. Geochem. Cosmochim. Acta 96, 57–79.

Deininger, M., Scholz, D., 2019. Isolution 1.0: an ISOtope evoLUTION model describing the stable oxygen (delta O-18) and carbon (delta C-1(3)) isotope values of speleothems. Int. J. Speleol. 48, 21–32.

deMenocal, P.B., 2001. Cultural responses to climate change during the late Holocene. Science 292, 667–673.

Demeny, A., Kele, S., Siklosy, Z., 2010. Empirical equations for the temperature dependence of calcite-water oxygen isotope fractionation from 10 to 70 degrees C. Rapid Commun. Mass Spectrom. 24, 3521–3526.

Denton, G.H., Alley, R.B., Comer, G.C., Broecker, W.S., 2005. The role of seasonality in abrupt climate change. Quat. Sci. Rev. 24, 1159–1182.

Dietzel, M., Tang, J.W., Leis, A., Kohler, S.J., 2009. Oxygen isotopic fractionation during inorganic calcite precipitation - effects of temperature, precipitation rate

and pH. Chem. Geol. 268, 107–115.
Domínguez-Villar, D., Fairchild, I.J., Baker, A., Wang, X.F., Edwards, R.L., Cheng, H., 2009. Oxygen isotope precipitation anomaly in the North Atlantic region during the 8.2 ka event. Geology 37, 1095–1098.
Domínguez-Villar, D., Wang, X., Cheng, H., Martin-Chivelet, J., Edwards, M.E., 2008. A high-resolution late Holocene speleothem record from Kaite Cave, northern Spain: $\delta^{18}O$ variability and possible causes. Quat. Int. 187, 40–51.
Domínguez-Villar, D., Wang, X., Krklec, K., Cheng, H., Edwards, R.L., 2017. The control of the tropical North Atlantic on Holocene millennial climate oscillations. Geology 45, 303–306.
Dominguez-Villar, D., Wang, X.F., Krklec, K., Cheng, H., Edwards, R.L., 2017. The control of the tropical North Atlantic on Holocene millennial climate oscillations. Or. Geol. 45, 303–306.
Dreybrodt, W., 2016. Comment on "Stoll H. et al. (2015): interpretation of orbital scale variability in mid-latitude speleothem delta O-18: significance of growth rate controlled kinetic fractionation effects. Quat. Sci. Rev. 127, 215-228". Quat. Sci. Rev. 142, 179–181.
Dreybrodt, W., 2019. Comment on "Maximilian Hansen, Denis Scholz, Bernd R. Schöne, Christoph Spötl, simulating speleothem growth in the laboratory: determination of the stable isotope fractionation (δ13C and δ18O) between H2O, DIC and CaCO3". Chem. Geol. 509, 20–44, 2019.
Drysdale, R., Zanchetta, G., Hellstrom, J., Maas, R., Fallick, A., Pickett, M., Cartwright, I., Piccini, L., 2006. Late Holocene drought responsible for the collapse of Old World civilizations is recorded in an Italian cave flowstone. Or. Geol. 34, 101–104.
Dykoski, C.A., Edwards, R.L., Cheng, H., Yuan, D.X., Cai, Y.J., Zhang, M.L., Lin, Y.S., Qing, J.M., An, Z.S., Revenaugh, J., 2005. A high-resolution, absolute-dated Holocene and deglacial Asian monsoon record from Dongge Cave, China. Earth Planet. Sci. Lett. 233, 71–86.
Epstein, S., Mayeda, T., 1953. Variation of O-18 content of waters from natural sources. Geochem. Cosmochim. Acta 4, 213–224.
Fairchild, I.J., Baker, A., 2012. Speleothem Science: from Processes to Past Environments. Wiley-Blackwell, Chichester, UK.
Fleitmann, D., Mudelsee, M., Burns, S.J., Bradley, R.S., Kramers, J., Matter, A., 2008. Evidence for a widespread climatic anomaly at around 9.2 ka before present. Paleoceanography 23.
Fohlmeister, J., Arps, J., Spotl, C., Schroder-Ritzrau, A., Plessen, B., Gunter, C., Frank, N., Trussel, M., 2018. Carbon and oxygen isotope fractionation in the water-calcite-aragonite system. Geochem. Cosmochim. Acta 235, 127–139.
Gabitov, R.I., Watson, E.B., Sadekov, A., 2012. Oxygen isotope fractionation between calcite and fluid as a function of growth rate and temperature: an in situ study. Chem. Geol. 306, 92–102.
Genty, D., Blamart, D., Ghaleb, B., Plagnes, V., Causse, C., Bakalowicz, M., Zouari, K., Chkir, N., Hellstrom, J., Wainer, K., Bourges, F., 2006. Timing and dynamics of the last deglaciation from European and North African delta C-13 stalagmite profiles - comparison with Chinese and South Hemisphere stalagmites. Quat. Sci. Rev. 25, 2118–2142.
Gimeno, L., Nieto, R., Trigo, R.M., Vicente-Serrano, S.M., Lopez-Moreno, J.I., 2010. Where does the Iberian peninsula moisture come from? An answer based on a Lagrangian approach. J. Hydrometeorol. 11, 421–436.
Grant, K.M., Rohling, E.J., Ramsey, C.B., Cheng, H., Edwards, R.L., Florindo, F., Heslop, D., Marra, F., Roberts, A.P., Tamisiera, M.E., Williams, F., 2014. Sea-level variability over five glacial cycles. Nat. Commun. 5, 1–9, 5076.
Grindley, J., 1969. The Calculation of Actual Evaporation and Soil Moisture deficit Over Specified catchment Areas. Meteorological Office, Hydrological Services.
Guo, W., Zhou, C., 2019. Patterns and controls of disequilibrium isotope effects in speleothems: insights from an isotope-enabled diffusion-reaction model and implications for quantitative thermometry. Geochem. Cosmochim. Acta 267, 196–226. https://doi.org/10.1016/j.gca.2019.07.028.
Hammer, O., Harper, D., Ryan, P., 2001. Paleontological statistics software package for education and data analysis. Palaeontol. Electron. 4, 9–18.
Hans Wedepohl, K., 1995. The composition of the continental crust. Geochem. Cosmochim. Acta 59, 1217–1232.
Hansen, M., Scholz, D., Schöne, B.R., Spötl, C., 2019. Simulating speleothem growth in the laboratory: determination of the stable isotope fractionation (δ13C and δ18O) between H2O, DIC and CaCO3. Chem. Geol. 509, 20–44.
Haug, G.H., Hughen, K.A., Sigman, D.M., Peterson, L.C., Rohl, U., 2001. Southward migration of the intertropical convergence zone through the Holocene. Science 293, 1304–1308.
Hoffmann, D.L., Prytulak, J., Richards, D.A., Elliott, T.R., Coath, C.D., Smart, P.L., Scholz, D., 2007. Procedures for accurate U and Th isotope measurements by high precision MC-ICPMS. Int. J. Mass Spectrom. Ion Process. 264, 97–109.
Hsiang, S.M., Burke, M., Miguel, E., 2013. Quantifying the influence of climate on human conflict. Science 341.
Isola, I., Zanchetta, G., Drysdale, R.N., Regattieri, E., Bini, M., Bajo, P., Hellstrom, J.C., Baneschi, I., Lionello, P., Woodhead, J., Greig, A., 2019. The 4.2 ka event in the central Mediterranean: new data from a Corchia speleothem (Apuan Alps, central Italy). Clim. Past 15, 135–151.
Jackson, A.S., 2009. Detecting Radiocarbon Fluctuations Using Stalagmites. Geological Sciences. University College Dublin, Dublin, p. 350.
James, E., Banner, J., Hardt, B., 2015. A Global Model for Cave Ventilation and Seasonal Bias in Speleothem Paleoclimate Records: A Global Model for Cave Ventilation.
Johnston, V.E., Borsato, A., Spotl, C., Frisia, S., Miorandi, R., 2013. Stable isotopes in caves over altitudinal gradients: fractionation behaviour and inferences for speleothem sensitivity to climate change. Clim. Past 9, 99–118.
Kennett, D.J., Breitenbach, S.F.M., Aquino, V.V., Asmerom, Y., Awe, J., Baldini, J.U.L., Bartlein, P., Culleton, B.J., Ebert, C., Jazwa, C., Macri, M.J., Marwan, N., Polyak, V., Prufer, K.M., Ridley, H.E., Sodemann, H., Winterhalder, B., Haug, G.H., 2012. Development and disintegration of Maya political systems in response to climate change. Science 338, 788.
Kim, S.-T., O'Neill, J.R., 1997. Equilibrium and nonequilibrium oxygen isotope effects in synthetic carbonates. Geochem. Cosmochim. Acta 61, 3461–3475.
Kim, S.T., O'Neil, J.R., Hillaire-Marcel, C., Mucci, A., 2007. Oxygen isotope fractionation between synthetic aragonite and water: influence of temperature and Mg2+ concentration. Geochem. Cosmochim. Acta 71, 4704–4715.
Lie, O., Paasche, O., 2006. How extreme was northern hemisphere seasonality during the Younger Dryas? Quat. Sci. Rev. 25, 404–407.
Lynch-Stieglitz, J., 2017. The Atlantic meridional overturning circulation and abrupt climate change. Annual Review Mar. Sci. 9, 83–104.
Martin-Chivelet, J., Munoz-Garcia, M.B., Edwards, R.L., Turrero, M.J., Ortega, A.I., 2011. Land surface temperature changes in Northern Iberia since 4000 yr BP, based on delta C-13 of speleothems. Glob. Planet. Chang. 77, 1–12.
Mary, Y., Eynaud, F., Colin, C., Rossignol, L., Brocheray, S., Mojtahid, M., Garcia, J., Peral, M., Howa, H., Zaragosi, S., Cremer, M., 2017. Changes in Holocene meridional circulation and poleward Atlantic flow: the Bay of Biscay as a nodal point. Clim. Past 13, 201–216.
Masson-Delmotte, V., Landais, A., Stievenard, M., Cattani, O., Falourd, S., Jouzel, J., Johnsen, S.J., Jensen, D.D., Sveinsbjornsdottir, A., White, J.W.C., Popp, T., Fischer, H., 2005. Holocene climatic changes in Greenland: different deuterium excess signals at Greenland ice core Project (GRIP) and NorthGRIP. J. Geophys. Res. Atmos. 110.
McDermott, F., 2004. Palaeo-climate reconstruction from stable isotope variations in speleothems: a review. Quat. Sci. Rev. 23, 901–918.
McDermott, F., Atkinson, T.C., Fairchild, I.J., Baldini, L.M., Mattey, D.P., 2011. A first evaluation of the spatial gradients in delta O-18 recorded by European Holocene speleothems. Glob. Planet. Chang. 79, 275–287.
McDermott, F., Baldini, L.M., Baldini, J.U.L., 2006. Forward modelling of speleothem delta O-18: a critical assessment of their use as high-resolution climate proxies. Geochem. Cosmochim. Acta 70, A408–a408.
McDermott, F., Schwarcz, H., Rowe, P.J., 2005. Isotopes in speleothems. In: Leng, M.J. (Ed.), Isotopes in Palaeoenviroenmental Research. Springer, Amsterdam, pp. 185–225.
Morellón, M., Aranbarri, J., Moreno, A., González-Sampériz, P., Valero-Garcés, B.L., 2018. Early Holocene humidity patterns in the Iberian Peninsula reconstructed from lake, pollen and speleothem records. Quat. Sci. Rev. 181, 1–18.
Morellon, M., Valero-Garces, B., Vegas-Vilarrubia, T., Gonzalez-Samperiz, P., Romero, O., Delgado-Huertas, A., Mata, P., Moreno, A., Rico, M., Corella, J.P., 2009. Lateglacial and Holocene palaeohydrology in the western Mediterranean region: the lake Estanya record (NE Spain). Quat. Sci. Rev. 28, 2582–2599.
Moreno, A., Perez-Mejias, C., Bartolome, M., Sancho, C., Cacho, I., Stoll, H., Delgado-Huertas, A., Hellstrom, J., Edwards, R.L., Cheng, H., 2017. New speleothem data from Molinos and Ejulve caves reveal Holocene hydrological variability in northeast Iberia. Quat. Res. 88, 223–233.
Moreno, A., Perez, A., Frigola, J., Nieto-Moreno, V., Rodrigo-Gamiz, M., Martrat, B., Gonzalez-Samperiz, P., Morellon, M., Martin-Puertas, C., Corella, J.P., Belmonte, A., Sancho, C., Cacho, I., Herrera, G., Canals, M., Grimalt, J.O., Jimenez-Espejo, F.J., Martinez-Ruiz, F., Vegas-Vilarrubia, T., Valero-Garces, B.L., 2012. The Medieval climate anomaly in the Iberian peninsula reconstructed from marine and lake records. Quat. Sci. Rev. 43, 16–32.
Moreno, A., Sancho, C., Bartolome, M., Oliva-Urcia, B., Delgado-Huertas, A., Estrela, M.J., Corell, D., Lopez-Moreno, J.I., Cacho, I., 2014. Climate controls on rainfall isotopes and their effects on cave drip water and speleothem growth: the case of Molinos cave (Teruel, NE Spain). Clim. Dyn. 43, 221–241.
Moreno, A., Stoll, H., Jimenez-Sanchez, M., Cacho, I., Valero-Garces, B., Ito, E., Edwards, R.L., 2010. A speleothem record of glacial (25-11.6 kyr BP) rapid climatic changes from northern Iberian Peninsula. Glob. Planet. Chang. 71, 218–231.
Morley, A., Schulz, M., Rosenthal, Y., Mulitza, S., Paul, A., Rühlemann, C., 2011. Solar modulation of North Atlantic central Water formation at multidecadal timescales during the late Holocene. Earth Planet. Sci. Lett. 308, 161–171.
Mühlinghaus, C., Scholz, D., Mangini, A., 2007. Modelling stalagmite growth and $\delta^{13}C$ as a function of drip interval and temperature. Geochem. Cosmochim. Acta 71, 2780–2790.
Müller, W., Shelley, M., Miller, P., Broude, S., 2009. Initial performance metrics of a new custom-designed ArF excimer LA-ICPMS system coupled to a two-volume laser-ablation cell. J. Anal. Atom. Spectrom. 24, 209–214.
Oliva, M., Ruiz-Fernandez, J., Barriendos, M., Benito, G., Cuadrat, J.M., Dominguez-Castro, F., Garcia-Ruiz, J.M., Giralt, S., Gomez-Ortiz, A., Hernandez, A., Lopez-Costas, O., Lopez-Moreno, J.I., Lopez-Saez, J.A., Martinez-Cortizas, A., Moreno, A., Prohom, M., Saz, M.A., Serrano, E., Tejedor, E., Trigo, R., Valero-Garces, B., Vicente-Serrano, S.M., 2018. The little ice age in Iberian mountains. Earth Sci. Rev. 177, 175–208.
Oliva, M., Serrano, E., Gomez-Ortiz, A., Gonzalez-Amuchastegui, M.J., Nieuwendam, A., Palacios, D., Perez-Alberti, A., Pellitero-Ondicol, R., Ruiz-Fernandez, J., Valcaarcel, M., Vieira, G., Antoniades, D., 2016. Spatial and temporal variability of periglaciation of the Iberian Peninsula. Quat. Sci. Rev. 137, 176–199.
Olsen, J., Anderson, N.J., Knudsen, M.F., 2012. Variability of the north Atlantic oscillation over the past 5,200 years. Nat. Geosci. 5, 808–812.

Ontañón, R., Arias, P., Gutiérrez Cuenca, E., Hierro Gárate, J., Etxeberria, F., Herrasti, L., Uzquiano, P., 2018. Chapter 8. Hidden in the Depths, Far from the People. Funerary Activities in the Lower Gallery of La Garma and the Use of Natural Caves as Burial Places in Early Medieval Cantabria, Northern Spain.

Pailler, D., Bard, É., 2002a. Geochemistry and sea-surface temperature reconstruction for sediment cores of the Iberian Margin, Supplement to: Pailler, D; Bard, É (2002): high frequency palaeoceanographic changes during the past 140000 yr recorded by the organic matter in sediments of the Iberian Margin. Palaeogeogr. Palaeoclimatol. Palaeoecol. 181 (4), 431–452. https://doi.org/10.1016/S0031-0182(01)00444-8.PANGAEA.

Pailler, D., Bard, É., 2002b. High frequency palaeoceanographic changes during the past 140 000 yr recorded by the organic matter in sediments of the Iberian Margin. Palaeogeogr. Palaeoclimatol. Palaeoecol. 181, 431–452.

Pérez-Brunius, P., Rossby, T., Watts, D.R., 2004. Absolute transports of mass and temperature for the north Atlantic current– subpolar front system. J. Phys. Oceanogr. 34, 1870–1883.

Pohlmann, H., Sienz, F., Latif, M., 2006. Influence of the multidecadal Atlantic meridional overturning circulation variability on European climate. J. Clim. 19, 6062–6067.

Railsback, L.B., Liang, F.Y., Romani, J.R.V., Grandal-d'Anglade, A., Rodriguez, M.V., Fidalgo, L.S., Mosquera, D.F., Cheng, H., Edwards, R.L., 2011. Petrographic and isotopic evidence for Holocene long-term climate change and shorter-term environmental shifts from a stalagmite from the Serra do Courel of northwestern Spain, and implications for climatic history across Europe and the Mediterranean. Palaeogeogr. Palaecol. 305, 172–184.

Rasmussen, S.O., Vinther, B.M., Clausen, H.B., Andersen, K.K., 2007. Early Holocene climate oscillations recorded in three Greenland ice cores. Quat. Sci. Rev. 26, 1907–1914.

Rodrigo, F.S., Esteban-Parra, M.J., Pozo-Vasquez, D., Castro-Diez, Y., 2000. Rainfall variability in southern Spain on decadal to centennial time scales. Int. J. Climatol. 20, 721–732.

Rossi, C., Bajo, P., Lozano, R.P., Hellstrom, J., 2018. Younger Dryas to Early Holocene paleoclimate in Cantabria (N Spain): constraints from speleothem Mg, annual fluorescence banding and stable isotope records. Quat. Sci. Rev. 192, 71–85.

Rudzka-Phillips, D., McDermott, F., Jackson, A., Fleitmann, D., 2013. Inverse modelling of the C-14 bomb pulse in stalagmites to constrain the dynamics of soil carbon cycling at selected European cave sites. Geochem. Cosmochim. Acta 112, 32–51.

Sherwin, C.M., Baldini, J.U.L., 2011. Cave air and hydrological controls on prior calcite precipitation and stalagmite growth rates: implications for palaeoclimate reconstructions using speleothems. Geochem. Cosmochim. Acta 75, 3915–3929.

Smart, P.L., Friederich, H., 1987. Water movement and storage in the unsaturated zone of a maturely karstified carbonate aquifer, Mendip Hills, England. In: Proceedings of the Environmental Problems in Karst Terranes and Their Solutions Conference, pp. 57–87. KY, USA.

Smith, A.C., Wynn, P.M., Barker, P.A., Leng, M.J., Noble, S.R., Tych, W., 2016. North Atlantic forcing of moisture delivery to Europe throughout the Holocene. Sci. Rep. 6.

Souza, P., Cavalcanti, I.F.A., 2009. Atmospheric centres of action associated with the Atlantic ITCZ position. Int. J. Climatol. 29, 2091–2105.

Stanley, J.D., Krom, M.D., Cliff, R.A., Woodward, J.C., 2003. Short contribution: nile flow failure at the end of the old kingdom, Egypt: strontium isotopic and petrologic evidence. Geoarchaeology 18, 395–402.

Staubwasser, M., Sirocko, F., Grootes, P.M., Segl, M., 2003. Climate change at the 4.2 ka BP termination of the Indus valley civilization and Holocene south Asian monsoon variability. Geophys. Res. Lett. 30.

Stoll, H., Mendez-Vicente, A., Gonzalez-Lemos, S., Moreno, A., Cacho, I., Cheng, H., Edwards, R.L., 2015. Interpretation of orbital scale variability in mid-latitude speleothem delta O-18: significance of growth rate controlled kinetic fractionation effects. Quat. Sci. Rev. 127, 215–228.

Stoll, H.M., Moreno, A., Banasiak, A., Jimenez-Sanchez, M., Cacho, I., Vadillo, I., Burns, S., Cuesta, M.J.D., Edwards, R.L., Cheng, H., 2009. Speleothem evidence for coupling between Iberian peninsula hydrology and North Atlantic oceanic and atmospheric modes. Geochem. Cosmochim. Acta 73. A1278-A1278.

Thornthwaite Jr., C.W., 1955. The Water Balance, vol. III. Publications in Climatology, Drexel Institute of Technology, Centerton, NJ.

Tremaine, D.M., Froelich, P.N., Wang, Y., 2011. Speleothem calcite farmed in situ: modern calibration of $\delta^{18}O$ and $\delta^{13}C$ paleoclimate proxies in a continuously-monitored natural cave system. Geochem. Cosmochim. Acta 75, 4929–4950.

Trigo, R.M., Pozo-Vazquez, D., Osborn, T.J., Castro-Diez, Y., Gamiz-Fortis, S., Esteban-Parra, M.J., 2004. North Atlantic oscillation influence on precipitation, river flow and water resources in the Iberian peninsula. Int. J. Climatol. 24, 925–944.

Trouet, V., Esper, J., Graham, N.E., Baker, A., Scourse, J.D., Frank, D.C., 2009. Persistent positive North Atlantic oscillation mode dominated the Medieval climate anomaly. Science 324, 78–80.

Trueba, J.J.G., Moreno, R.M., de Pison, E.M., Serrano, E., 2008. 'Little ice age' glaciation and current glaciers in the Iberian peninsula. Holocene 18, 551–568.

Walczak, I.W., Baldini, J.U.L., Baldini, L.M., McDermott, F., Marsden, S., Standish, C.D., Richards, D.A., Andreo, B., Slater, J., 2015. Reconstructing high-resolution climate using CT scanning of unsectioned stalagmites: a case study identifying the mid-Holocene onset of the Mediterranean climate in southern Iberia. Quat. Sci. Rev. 127, 117–128.

Walker, M.J.C., Berkelhammer, M., Björck, S., Cwynar, L.C., Fisher, D.A., Long, A.J., Lowe, J.J., Newnham, R.M., Rasmussen, S.O., Weiss, H., 2012. Formal subdivision of the Holocene series/epoch: a discussion paper by a working group of INTIMATE (integration of ice-core, marine and terrestrial records) and the subcommission on quaternary Stratigraphy (international commission on Stratigraphy). J. Quat. Sci. 27, 649–659.

Wirth, S.B., Glur, L., Gilli, A., Anselmetti, F.S., 2013. Holocene flood frequency across the Central Alps - solar forcing and evidence for variations in North Atlantic atmospheric circulation. Quat. Sci. Rev. 80, 112–128.